Taylor & Francis
Taylor & Francis Group

Mechanics of Advanced Materials and Structures

ISSN: 1537-6494 (Print) 1537-6532 (Online) Journal homepage: https://www.tandfonline.com/loi/umcm20

Free vibration analysis of variable stiffness laminated composite beams

Z. Kheladi, Sidi Mohammed Hamza-Cherif & M. E. A. Ghernaout

To cite this article: Z. Kheladi, Sidi Mohammed Hamza-Cherif & M. E. A. Ghernaout (2020): Free vibration analysis of variable stiffness laminated composite beams, Mechanics of Advanced Materials and Structures, DOI: 10.1080/15376494.2020.1712750

To link to this article: https://doi.org/10.1080/15376494.2020.1712750

Published online: 30 Jan 2020.

MECHANICS OF ADVANCED MATERIALS AND STRUCTURES
https://doi.org/10.1080/15376494.2020.1712750

Taylor & Francis
Taylor & Francis Group

ORIGINAL ARTICLE

Free vibration analysis of variable stiffness laminated composite beams

Z. Kheladi, Sidi Mohammed Hamza-Cherif, and M. E. A. Ghernaout

Mecacomp Laboratory, Department of Mechanical Engineering, Faculty of Technology, University of Tlemcen, Tlemcen, Algeria

ABSTRACT

In this paper, the free vibration analysis of composite laminated beams reinforced with parabolic fibers are studied on the basis of the equivalent single layer theory (ESLT) using the isogeomtric analysis method. In the composite material with variable stiffness (VSCL), each layer is reinforced by curvilinear fiber, while in the traditional composite materials with constant stiffness (CSCL) each layer is reinforced by straight fiber. The Equivalent Single Layer Theory (ESLT) given by the Continuum-based Timoshenko beam theory (CTBT) is combined with the isogeometric analysis, in which twisting and stretching effects are considered. The differential equations of motion governing the dynamics of stretching, shearing, bending and twisting composite beam are derived using the Hamilton principle. A new isogeometric composite beam element with six degrees of freedom per control point is developed and used to find natural frequencies of variable stiffness composites beams with parabolic fibers. In this new model, the effects of transverse shear deformation, rotary inertia, and the coupling effect due to the lamination of composite layers are included. Results are obtained for a number constant stiffness composite beam. The results confirm that the solutions converge as the number of elements or the degrees of basic functions are increased. Highly accurate values are obtained with the use of a very few degrees of freedoms, in which h-, p- and k-refinement are used in the convergence analysis. New numerical results of comparison study between the variable stiffness composite beams and constant stiffness composite beams are investigated. Next, parametric study is presented to investigate the impact of orientation angle of parabolic fiber, the stacking sequences, number of layers, boundary conditions, modulus ratio and length to mean diameter ratios on the natural frequencies of the variable stiffness composite beams. The solutions of variable stiffness composite beams are provided as benchmark for future studies.

ARTICLE HISTORY
Received 26 November 2019
Accepted 5 January 2020

KEYWORDS
Variable stiffness composite beam; parabolic fibers; ESLT theory; IGA; free vibration

1. Introduction

Composite materials have been widely used in many engineering fields such as mechanical manufacturing, aeronautical, civil, transportation, and marine due to various benefits like to lightness, high strength-to- weight, stiffness-to- weight ratios, high resistance to corrosion and fatigue, etc.

The studies of free vibration of laminated composite beams has gained increasing importance, due to the increasing use of these structures in many areas of engineering such as automotive, aeronautic, nuclear, etc. For these purposes, many authors have contributed to develop mathematical and numerical models based on beam theories, see for instance [1–11]. We can mention among others the model developed by Patrick and Cunniff [12], they studied the free vibration of composite cantilever beam reinforced with unidirectional fibers. Several experimental tests were performed in order to predict the natural frequencies and the mode shapes of various examples of composite beam with different fiber orientations angle ($0°, 15°$, $30°$ and $90°$). Also, the authors developed a numerical model to predict the behavior of a composite beam. The bending-torsion coupling and the transverse shear effects with rotary inertia have been incorporated in the model. The elastic constants used in this numerical model were experimentally determined. Good accuracy has been obtained between the numerical and experimental solution. They concluded that the coupling bending and twisting have a good interaction for certain values in the case of laminates $(15^{\circ}, 30^{\circ})$ and have an influence on the frequency values. Teoh and Huang [13] treated the free vibration of composite beams based on a continuous model by using the analytical solution. The model has included the shear deformation and rotary inertia effects. They investigated that is much more suitable for predicting the behavior of a composite beams, and the natural frequencies that are influenced when the shear deformation and rotary inertia effects become large. These last authors [14] treated in another study the relation between the torsion-flexure coupling effect and the effect of orientation fibers on normal mode shapes. They concluded that the change of the fiber orientations lead to changing the coupling effects and showed that the coupling effects are of most importance especially when the orientation fibers become less them 25 degree. Yildirim [15] studied the influence of the longitudinal to transverse modulus ratio on the in-plane natural frequencies of symmetric cross-ply composite beams. First order shear deformation theory (FSDT) was used for modeling the composite beam using the stiffness method, which takes into account the transverse and axial shear deformation and rotary inertia effects.

CONTACT Z. Kheladi zakikheladi@gmail.com Mecacomp Laboratory, Department of Mechanical Engineering, Faculty of Technology, University of Tlemcen, Tlemcen, 13000 Algeria.
Color versions of one or more of the figures in the article can be found online at www.tandfonline.com/umcm.

The effect of thickness-length ratios and the boundary conditions on the beams in-plane mode shapes is studied.

Rajeshkumar and Hariharan [16] used the combinations of hybrid composites materials (carbon/epoxy and Glass/epoxy) to analyze the vibration of beams using the software (FEM-ANSYS 12.0). They investigated that the natural frequencies and the mode shapes of hybrid composite beams obtained under the effects of orientation fibers and aspect ratios are much more than the ordinary composites. Khatri et al. [17] studied the effect of various mechanical properties such as tensile strength, flexural strength, impact of strength and young's modulus on the vibration of composite beams. They found that the natural frequencies of composite beam by using analytical method and the software ANSYS based on the finite element method.

Composite materials with variable stiffness (VSCL) are currently growing at a rate well above that of Composite materials with constant stiffness (CSLC) as a whole. In the composite material with variable stiffness, each layer is reinforced by curvilinear fiber, while in the traditional composite materials with constant stiffness each layer is reinforced by straight fiber. This variation in stiffness has very higher properties than conventional materials; lightness, high strength and rigidity, high resistance to fatigue, etc.

The study of behavior of structures constructed using the variable stiffness composite materials has been the subject of many researches. Martin and leissa [18] studied the vibration of variable stiffness composite plates subjected to buckling effect by the Ritz method. They showed that the buckling performance is improved using the new concept of composite materials. Hyer and lee [19] verified the buckling performance of plates reinforced with curvilinear fibers using the finite element analysis. Honda et al. [20] employed the Ritz method in order to analyze the vibration of plates reinforced with parabolic fibers. They determined the natural frequencies and modes shapes of plates for differences boundary conditions. The same authors [21] applied in another study the optimum design method to construct a new types of curved fibers using the FEM.

Ribeiro et coworkers [22–26] have applied the hierarchical finite element method for improving the behavior of variable stiffness laminated composite plates in several cases of linear and non-linear vibration, buckling performance, and safety factors, based on the first order shear deformation, the third order deformation and zig-zag layer wise theories respectively. They concluded that the results obtained have a high performance than the results of traditional composite materials. Houmat [27] studied the free vibration of VSCL symmetrical and anti-symmetrical plates based on the classical plates theory using the p-version of finite elements method. He showed that the anti-symmetrical configuration improved the linear and non-linear natural frequencies than the symmetrical configurations. Hachemi et al. [28] used the first order shear deformation theory for studying the free vibration of perforated composite plates reinforced with parabolic fibers using the HFEM. Serdoun and Hamza-cherif [29], Hachemi [30], studied the vibration of sandwich composite plates reinforced with parabolic fibers based on the HSDT-C^1 and HSDT-C° theories respectively where both used the p-version of finite element method. Bendahmane et al. [31] employed the HFEM for improving the performance of the VSCL plates immersed in fluid based on higher-order C° theory. Researches on the vibration of composite beams with variable stiffness are very limited. Zamani et al. [32] suggested a design of thin-walled composite beams reinforced with curvilinear fibers to improve the performance of beams behavior subjected to different loading with various physical and mechanical parameters. Haddadpour and Zamani [33] developed an aeroelastic design for composite wings. Boukhalfa [34] studied the free vibration of a rotating composite shaft with curvilinear fibers. The p- version of the finite element method is adopted to study the problem based on the CTBT theory. The results were presented in the form of Campbell diagrams.

The finite element method is considered as one of the most versatile and powerful numerical methods applied to beams-dynamics. Compared to the analytical methods the FEM can treat complex problems in which the effects: transverse shear deformation, rotary inertia and gyroscopic effects, laminate coupling mechanism, internal and external damping, supports stiffness, fiber orientation and stacking sequence can be introduced. Many investigators have suggested various finite element (FE) models for the analysis of composite beams; however, beam elements (h and p version) represent one of the basic components in rotor-dynamics.

It is well known that the standard finite element method is based on polynomial approximation this will inevitably lead to discretization errors. In addition, the FE model is only an approximation of the original computer-aided design (CAD) model, this lead automatically to the lack of accuracy. Hughes et al. [35, 36] suggested a novel approach called Isogeometric Analysis (IGA). The first goal of this approach is to fill the gap between the finite element method and computer aided design CAD, which is described by Non-Uniform Rational B-splines (NURBS). It essentially utilizes the same basis functions to represent the geometry as well as to approximate the solution field, seeking to create a single discretization. For these purposes, several papers of parameterization based on the free-form B-spline approximations in combination with various laser-based measurement technologies have been presented in the few last year's [37–41], for improving the results of deformation analysis of composite structures. A number of studies has been performed over the past few years using this approach and showed that IGA offer many advantages and appealing features better than classical FEM, it include high-order continuity of basic functions, which further leads to more stable numerical conditioning, exhibits very convenient convergence rates especially in vibrational behavior analysis and a better integration into the CAE process.

The IGA has been successfully applied for the solution of many kinds of engineering problems, for instance structural vibration [42], beams analysis [43, 45], plates and shells analysis [46–52], and optimization [53, 54], etc. A detailed introduction into IGA and summary of properties and applications can be found in the monograph [36].

The Few number of publications carried out to vibrations of laminated composite structures with curvilinear fibers were combined with IGA. Hao et al. [55] applied the isogeometric method in combination with the Reissner–Mindlin plates theory for buckling analysis of variable-stiffness laminated plates. Khalafi and Fazilati [56] studied the free vibrations and characteristics

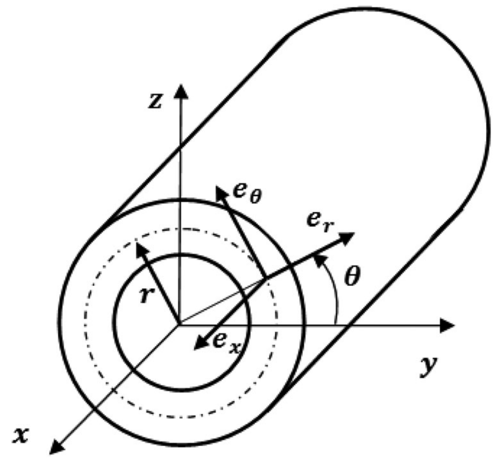

Figure 1. Coordinate systems: Cartesian (x, y, z) and Cylindrical (x, r, θ).

linear flutter of asymmetric curvilinear laminates skew plates using the isogeometric analysis approach. The latter authors [57] investigate the optimization of aeroelastic flutter linear behavior of plates made of a variable stiffness composite laminates using the genetic algorithm based on the isogeometric analysis. In another study, Khalafi and Fazilati [58] used the isogeometric approach to evaluate the thresholds parametric instability of variable stiffness composite plates with subjected to uniform plane-loads. Khalafi and Fazilati [59] have been treated the problems of free vibrations of VSCL plates with various forms of cutout using isogeometric approach based on FSDT. Peng Hao et al. [60] studied the vibration of variable stiffness panels with cutout by isogeometric approach. Venkatachari et al. [61] presented a study on the free vibration of cylindrical and elliptical shells with VSCL using the isogeometric approach. The natural frequencies and modes are determined and compared with frequency and modes in constant stiffness (CSCL). Research has clearly shown that there is yet no work on the development and application of the isogeometric analysis method for the linear vibration problems of beams reinforced with parabolic fibers is not emerged.

Within this context, an extended Equivalent Single Layer Theory (ESLT) formulation of Chang et al. [9], Boukhalfa et al. [8], ben Arab [11], Boukhalfa [34] in combination with the isogeometric analysis method is proposed to study the free vibration of variable stiffness composite beams. In addition to the shear-normal coupling given by ESL [11], the twisting and stretching are added to the model. The latter also includes the effect of the transverse shear deformation, rotary inertia, and the coupling effect due to the lamination of composite layers, fiber orientation angle and stacking sequence. A new isogeometric composite beam element with six degrees of freedom per control point is developed. The convergence rate of the present isogeometric composite beam element is demonstrated by using h-, p- and k-refinements. The results of IGA are compared with data previously published in the literature for Hierarchical FEM, classical FEM and analytical solutions. The effects of material properties, orientation angles of parabolic fibers, stacking sequence of layers, length to mean diameter ratios, modulus elasticity ratio E_1/E_2, and boundary conditions on the natural frequencies of the composite beams are considered. Lastly, the present benchmark test solutions are provided as a future reference solution.

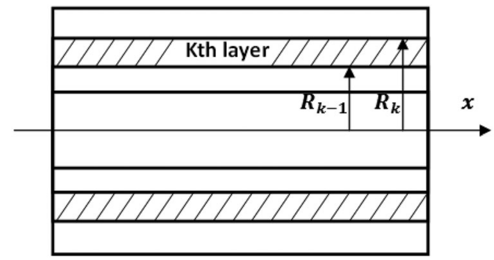

Figure 2. The kth layer of the composite beam.

2. Formulation

Energy formulation for a variable stiffness composite beam

The laminate VSCL beam is considered in this study with a circular cross section, Let x, y and z be the principle material coordinates of a shaft made of orthotropic material, and set x be the coordinate in the longitudinal axis.

In accordance with the first order shear deformation theory, the displacement field of an arbitrary point of the cross section of the beam in x, y and z directions can be expressed as:

$$\begin{aligned} U_x(x,y,z,t) &= u(x,t) + z\beta_x(x,t) - y\beta_y(x,t) \\ V_y(x,y,z,t\ ) &= v(x,t) - z\beta_z(x,t) \\ W_z(x,y,z,t) &= w(x,t) + y\beta_z(x,t) \end{aligned} \tag{1}$$

where U_x, V_y and W_z are the displacements of any point on the cross-section following the three axes x, y and z, respectively. As shown in Figure 1, the variable $u(x,t)$ denotes extensional displacement in x direction, while $v(x,t)$ and $w(x,t)$ are respectively the flexural displacements in y and z directions of the generic point on the reference axis of the beam. The variables $\beta_z(x,t)$, $\beta_x(x,t)$ and $\beta_y(x,t)$ denote respectively the rotation angles of the cross section about x, y and z axis.

The linear strain–displacement relationships can be expressed as:

$$\begin{Bmatrix} \varepsilon_{xx} \\ \gamma_{xy} \\ \gamma_{xz} \end{Bmatrix} = [L] \begin{Bmatrix} u \\ v \\ w \\ \beta_x \\ \beta_y \\ \beta_z \end{Bmatrix} \tag{2}$$

$$\varepsilon_{yy} = \varepsilon_{zz} = \gamma_{yz} = 0$$

The three strain components ε_{yy}, ε_{zz} and γ_{yz} being equal to zero is an assumption of the first order shear deformation theory, which does not consider transverse normal and shear deformation.where $[L]$ is the matrix of differential operators

$$[L] = \begin{bmatrix} \frac{\partial}{\partial x} & 0 & 0 & z\frac{\partial}{\partial x} & -y\frac{\partial}{\partial x} & 0 \\ 0 & \frac{\partial}{\partial x} & 0 & -1 & 0 & -z\frac{\partial}{\partial x} \\ 0 & 0 & \frac{\partial}{\partial x} & 1 & 0 & y\frac{\partial}{\partial x} \end{bmatrix} \tag{3}$$

As shown in Figure 1, the stress–strain relations of the composite beam of circular cross section can be expressed in the cylindrical coordinate system $(x, r,\ \theta)$ with unit vectors $(e_x,\ e_r,\ e_\theta)$ as

$$\begin{Bmatrix} \varepsilon_{xx} \\ \varepsilon_{\theta\theta} \\ \varepsilon_{rr} \\ \gamma_{x\theta} \\ \gamma_{r\theta} \\ \gamma_{xr} \end{Bmatrix} = \begin{bmatrix} 1 & 0 & 0 & 0 & 0 & 0 \\ 0 & \sin^2\theta & \cos^2\theta & 0 & -2\cos\theta\sin\theta & 0 \\ 0 & \cos^2\theta & \sin^2\theta & 0 & 2\cos\theta\sin\theta & 0 \\ 0 & 0 & 0 & -\sin\theta & 0 & \cos\theta \\ 0 & -\cos\theta\sin\theta & \cos\theta\sin\theta & 0 & (\cos^2\theta - \sin^2\theta) & 0 \\ 0 & 0 & 0 & \cos\theta & 0 & \sin\theta \end{bmatrix} \begin{Bmatrix} \varepsilon_{xx} \\ \varepsilon_{yy} \\ \varepsilon_{zz} \\ \gamma_{xy} \\ \gamma_{yz} \\ \gamma_{xz} \end{Bmatrix} \quad (4)$$

Since$\varepsilon_{yy} = \varepsilon_{zz} = \gamma_{yz} = 0$, the strain components in the cylindrical coordinate system can be simplified as follows:

$$\begin{Bmatrix} \varepsilon_{xx} \\ \gamma_{x\theta} \\ \gamma_{xr} \end{Bmatrix} = [R] \begin{Bmatrix} \varepsilon_{xx} \\ \gamma_{xy} \\ \gamma_{xz} \end{Bmatrix} \quad (5)$$

where the matrix of transformation $[R]$ from cylindrical coordinate system to Cartesian coordinate system is given by

$$[R] = \begin{bmatrix} 1 & 0 & 0 \\ 0 & -\sin\theta & \cos\theta \\ 0 & \cos\theta & \sin\theta \end{bmatrix} \quad (6)$$

Therefore, the strain components in the cylindrical coordinate system can be written in terms of the displacements and rotations variables as

$$\begin{Bmatrix} \varepsilon_{xx} \\ \gamma_{x\theta} \\ \gamma_{xr} \end{Bmatrix} = [R][L] \begin{Bmatrix} u \\ v \\ w \\ \beta_x \\ \beta_y \\ \beta_z \end{Bmatrix} \quad (7)$$

The constitutive stresses-strains relationships for kth layer (see Figure 2) defined by the inner radius R_{k-1} and outer radius R_k, in the orthotropic local coordinate (1–3), as shown in Figure 3, are expressed as

$$\begin{Bmatrix} \sigma_{11} \\ \sigma_{22} \\ \sigma_{33} \\ \tau_{23} \\ \tau_{13} \\ \tau_{12} \end{Bmatrix}^k = [Q]^k \begin{Bmatrix} \varepsilon_{11} \\ \varepsilon_{22} \\ \varepsilon_{33} \\ \gamma_{23} \\ \gamma_{13} \\ \gamma_{12} \end{Bmatrix}^k \quad (8)$$

where

$$[Q]^k = \begin{bmatrix} Q_{11} & Q_{12} & Q_{13} & 0 & 0 & 0 \\ Q_{12} & Q_{22} & Q_{23} & 0 & 0 & 0 \\ Q_{13} & Q_{23} & Q_{33} & 0 & 0 & 0 \\ 0 & 0 & 0 & Q_{44} & 0 & 0 \\ 0 & 0 & 0 & 0 & Q_{55} & 0 \\ 0 & 0 & 0 & 0 & 0 & Q_{66} \end{bmatrix}^k \quad (9)$$

Here, σ_i is stresses and ε_i is strain, the elasticity constants Q_{ij} are expressed in function of material properties, like Young's modulus E_i, Poisson's ratio ν_{ij} and shear modulus of the lamina G_{ij} and are defined as:

$$\begin{gathered} Q_{11} = \frac{E_{11}}{1-\nu_{12}\nu_{21}} \\ Q_{22} = \frac{E_{22}}{1-\nu_{12}\nu_{21}} \\ Q_{12} = \nu_{12}\frac{E_{22}}{1-\nu_{12}\nu_{21}} \\ Q_{66} = G_{12};\ Q_{44} = G_{23};\ Q_{55} = G_{13} \end{gathered} \quad (10)$$

where index 1 represents the directions parallel to the fibers direction, index 2 represents the in-plane direction perpendicular to the fibers direction. Index 3 is also perpendicular to the fiber direction, but is out-of-plane.

Let consider an arbitrary layer of the laminate whose fiber orientation makes an angle φ with respect to the x axis of the cylindrical coordinate system (x, r, θ) as shown in Figure 4.

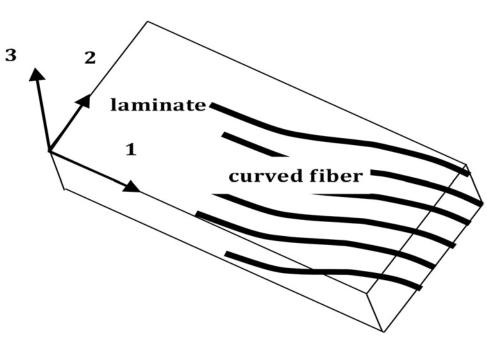

Figure 3. Orthotropic local coordinate (1, 2, 3).

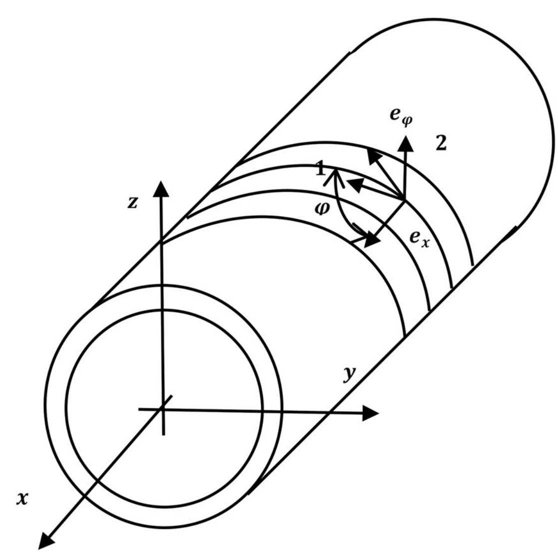

Figure 4. Composite beam and parabolic fiber orientation angle.

The stresses and strains from the orthotropic local coordinate system (1–3) should be transformed to cylindrical coordinate system (x, r, θ) by

$$\begin{Bmatrix} \sigma_{xx} \\ \sigma_{\theta\theta} \\ \sigma_{rr} \\ \tau_{r\theta} \\ \tau_{xr} \\ \tau_{x\theta} \end{Bmatrix}^k = [T]^k \begin{Bmatrix} \sigma_{11} \\ \sigma_{22} \\ \sigma_{33} \\ \tau_{23} \\ \tau_{13} \\ \tau_{12} \end{Bmatrix}^k \tag{11}$$

and

$$\begin{Bmatrix} \varepsilon_{11} \\ \varepsilon_{22} \\ \varepsilon_{33} \\ \gamma_{23} \\ \gamma_{13} \\ \gamma_{12} \end{Bmatrix}^k = [T]^{k^T} \begin{Bmatrix} \varepsilon_{xx} \\ \varepsilon_{\theta\theta} \\ \varepsilon_{rr} \\ \gamma_{r\theta} \\ \gamma_{xr} \\ \gamma_{x\theta} \end{Bmatrix}^k \tag{12}$$

where the transformation matrix $[T]$ is given by:

$$[T] = \begin{bmatrix} m^2 & n^2 & 0 & 0 & 0 & -2mn \\ n^2 & m^2 & 0 & 0 & 0 & 2mn \\ 0 & 0 & 1 & 0 & 0 & 0 \\ 0 & 0 & 0 & m & n & 0 \\ 0 & 0 & 0 & -n & m & 0 \\ mn & -mn & 0 & 0 & 0 & (m^2 - n^2) \end{bmatrix} \tag{13}$$

where $m = \cos\varphi, \;\; n = \sin\varphi$
From the two previous equations, the constitutive stresses-strains relationships for kth layer, in the cylindrical coordinate system (x, r, θ) are expressed as

$$\begin{Bmatrix} \sigma_{xx} \\ \sigma_{\theta\theta} \\ \sigma_{rr} \\ \tau_{r\theta} \\ \tau_{xr} \\ \tau_{x\theta} \end{Bmatrix}^k = \left[\overline{Q}\right]^k \begin{Bmatrix} \varepsilon_{xx} \\ \varepsilon_{\theta\theta} \\ \varepsilon_{rr} \\ \gamma_{r\theta} \\ \gamma_{xr} \\ \gamma_{x\theta} \end{Bmatrix}^k \tag{14}$$

where $\left[\overline{Q}\right]^k$ is the transformed material matrix, given by

$$\left[\overline{Q}\right]^k = [T]^k [Q]^k [T]^{k^T} = \begin{bmatrix} \overline{Q}_{11} & \overline{Q}_{12} & \overline{Q}_{13} & 0 & 0 & \overline{Q}_{16} \\ \overline{Q}_{12} & \overline{Q}_{22} & \overline{Q}_{23} & 0 & 0 & \overline{Q}_{26} \\ \overline{Q}_{13} & \overline{Q}_{23} & \overline{Q}_{33} & 0 & 0 & \overline{Q}_{36} \\ 0 & 0 & 0 & \overline{Q}_{44} & \overline{Q}_{45} & 0 \\ 0 & 0 & 0 & \overline{Q}_{45} & \overline{Q}_{55} & 0 \\ \overline{Q}_{16} & \overline{Q}_{26} & \overline{Q}_{36} & 0 & 0 & \overline{Q}_{66} \end{bmatrix}^k \tag{15}$$

The coefficients of transformed stiffness matrix $\overline{Q}_{ij}$ are expressed in terms of lamination angle φ and the stiffness matrix $\overline{Q}_{ij}$, the relations are given in the next section.

The Variable stiffness laminate composite beam with parabolic fiber is used in this study, in which the shape of fibers is differ than straight fibers, this implies that the orientations of fibers are changed at any point along the ply, which means that the values of transformed reduced stiffness elements of the matrix are not constant and become function of x.

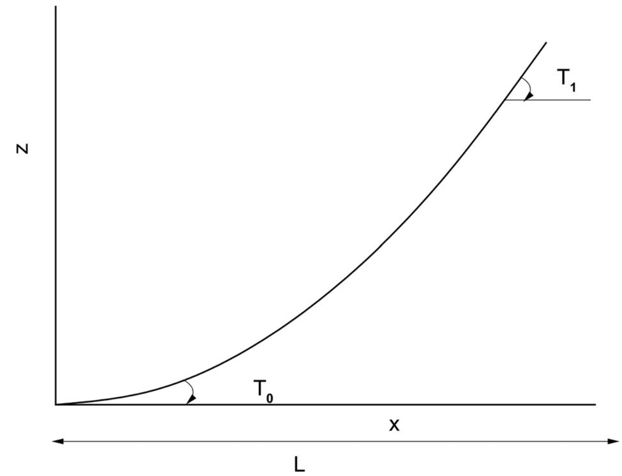

Figure 5. The configuration of variable stiffness composite beam with parabolic fiber.

The first element of matrix $\left[\overline{Q}_{11}\right]$ is written as:

$$\begin{aligned} \overline{Q}_{11} = {} & \cos^4\varphi(x) + Q_{22}\sin\varphi(x) \\ & + 2(Q_{12} + 2Q_{66})\sin^2\varphi(x)\cos^2\varphi(x) \end{aligned} \tag{16}$$

where $\varphi(x)$ is the fiber orientation angle of the VSCL beam. The others elements of matrices $\overline{Q}_{ij}$ are defined in the next.in this study, it is presupposed that the fiber path variation is parabolic shape.

$$f(x) = A\left(x - \frac{L}{2}\right)^2 \tag{17}$$

where A is the constant of proportionality of a parabola, given by:

$$A = \frac{\gamma L}{2} \tag{18}$$

in which, the shape of parabola is controlled by a non-dimensional parameter called γ in addition, L is the length of the beam.

By using the first derivative of the function f(x), the parabolic fiber path orientation angle can be written as

$$\varphi(x) = \tan^{-1}\left[\gamma(b - Lx)\right] \tag{19}$$

The fiber path orientation for the first and the second angles are defined respectively by angle T_0 and angle T_1, where the parabolic fiber orientation is assumed to vary with x from the fiber orientation angle T_0 at the beam center to T_1 at distance L from the center as shown in Figure 5, in which the configuration of the fibers orientation is denoted in this study by $[\langle T_0,\ T_1\rangle]$.

Inserting Eq. (19) into the $\left[\overline{Q}\right]$ is the transformed material matrix gives

$$\overline{Q}_{11} = \frac{Q_{11} + \gamma(b - Lx)Q_{22} - \gamma(b - Lx)2(Q_{12} + 2Q_{66})}{\left(\gamma^2 L^2 x^2 - 2\gamma^2 Lxb + \gamma^2 b^2 + 1\right)^2} \tag{20}$$

$$\overline{Q}_{16} = \frac{(Q_{11} - Q_{12} + 2Q_{66})\gamma(b - Lx) - \gamma(b - Lx)(Q_{12} - Q_{22} + 2Q_{66})}{(\gamma^2L^2x^2 - 2\gamma^2Lxb + \gamma^2b^2 + 1)^2} \tag{21}$$

$$\overline{Q}_{66} = \frac{(Q_{11} + Q_{22} - 2(Q_{12} + Q_{66}))\gamma(b - Lx) + Q_{66}(1 - \gamma(b - Lx))}{(\gamma^2L^2x^2 - 2\gamma^2Lxb + \gamma^2b^2 + 1)^2} \tag{22}$$

$$\overline{Q}_{55} = \frac{Q_{55} + \gamma(b - Lx)Q_{44}}{\left(1 + \left(\gamma(b - Lx)\right)^2\right)} \tag{23}$$

The transverse shear correction factor k_s is introduced to account for the approximation of the nonlinear distribution of transverse shear strains along the beam thickness. In the hypothesis that $\varepsilon_{\theta\theta} = \varepsilon_{rr} = \gamma_{r\theta} = 0$, the stress–strain relations become

$$\begin{Bmatrix} \sigma_{xx} \\ \tau_{x\theta} \\ \tau_{xr} \end{Bmatrix}^k = \left[\overline{Q}^*\right]^k \begin{Bmatrix} \varepsilon_{xx} \\ \gamma_{x\theta} \\ \gamma_{xr} \end{Bmatrix}^k \tag{24}$$

where $\left[\overline{Q}^*\right]^k$ is the modified transformed material matrix, given by

$$\left[\overline{Q}^*\right]^k = \begin{bmatrix} \overline{Q}_{11} & k_s\overline{Q}_{16} & 0 \\ k_s\overline{Q}_{16} & k_s\overline{Q}_{66} & 0 \\ 0 & 0 & k_s\overline{Q}_{55} \end{bmatrix}^k \tag{25}$$

in which, k_s represents the transverse shear correction factor.

Inserting Eq. (7) into Eq. (24) gives

$$\begin{Bmatrix} \sigma_{xx} \\ \tau_{x\theta} \\ \tau_{xr} \end{Bmatrix}^k = \left[\overline{Q}^*\right]^k [R][L] \begin{Bmatrix} u \\ v \\ w \\ \beta_x \\ \beta_y \\ \beta_z \end{Bmatrix} \tag{26}$$

The strain energy of a composite beam with parabolic fiber U is given by:

$$U = \frac{1}{2}\int_V \varepsilon^T\sigma \; dV \tag{27}$$

$$U = \frac{1}{2}\int_V (\sigma_{xx}\varepsilon_{xx} + \sigma_{rr}\varepsilon_{rr} + \sigma_{\theta\theta}\varepsilon_{\theta\theta} + \tau_{xr}\gamma_{xr} + \tau_{x\theta}\gamma_{x\theta} + \tau_{r\theta}\gamma_{r\theta})dV \tag{28}$$

Since$\varepsilon_{\theta\theta} = \varepsilon_{rr} = \gamma_{r\theta} = 0$, the strain energy U can be reduced to

$$U = \frac{1}{2}\int_V (\sigma_{xx}\varepsilon_{xx} + \tau_{xr}\gamma_{xr} + \tau_{x\theta}\gamma_{x\theta})dV \tag{29}$$

Using Eq. (24), the strain energy can be written as:

$$U = \frac{1}{2}\int_V \left(\overline{Q}_{11}{\varepsilon_{xx}}^2 + k_s\overline{Q}_{55}{\gamma_{xr}}^2 + k_s\overline{Q}_{66}{\gamma_{x\theta}}^2 + 2k_s\overline{Q}_{16}\varepsilon_{xx}\gamma_{x\theta}\right)dV \tag{30}$$

Replacing the relations for the cross section rotation where $y = r\cos\theta$ and $z = r\sin\theta$ as show in Figure 1, and integrating over the beam cross sectional area by summing up the contribution of each orthotropic layer, the general expression of the strain energy is given by:

$$\begin{aligned} U = {} & \frac{1}{2}A_{11}\int_0^L \left(\frac{\partial u}{\partial x}\right)^2 dx \\ & + \frac{1}{2}D_{11}\left[\int_0^L \left(\frac{\partial \beta_x}{\partial x}\right)^2 dx + \int_0^L \left(\frac{\partial \beta_y}{\partial x}\right)^2 dx\right] \\ & + \frac{1}{2}k_sB_{16}\left[2\int_0^L \frac{\partial \beta_z}{\partial x}\frac{\partial u}{\partial x}dx + \int_0^L \beta_y\frac{\partial \beta_x}{\partial x}dx - \int_0^L \beta_x\frac{\partial \beta_y}{\partial x}dx\right. \\ & \left. - \int_0^L \frac{\partial v}{\partial x}\frac{\partial \beta_x}{\partial x}dx - \int_0^L \frac{\partial w}{\partial x}\frac{\partial \beta_y}{\partial x}dx\right] \\ & + \frac{1}{2}k_s(A_{66} + A_{55})\left[\int_0^L \left(\frac{\partial v}{\partial x}\right)^2 dx + \int_0^L \left(\frac{\partial w}{\partial x}\right)^2 dx\right. \\ & \left. + \int_0^L {\beta_x}^2dx + \int_0^L {\beta_y}^2dx + 2\int_0^L \beta_x\frac{\partial w}{\partial x}dx - 2\int_0^L \beta_y\frac{\partial v}{\partial x}dx\right] \\ & + \frac{1}{2}k_sD_{66}\int_0^L \left(\frac{\partial \beta_z}{\partial x}\right)^2 dx, \end{aligned} \tag{31}$$

The constants $A_{i,j}$, $B_{i,j}$ are expressed in Appendix A.1, where L is the length of the beam. Next, the kinetic energy of the VSCL beam will be derived. The kinetic energy of the laminated beam including the effects of translatory and rotary inertia ones can be written as:

$$\begin{aligned} T = {} & \frac{1}{2}\int_0^L I_m\left[\left(\frac{\partial u}{\partial t}\right)^2 + \left(\frac{\partial v}{\partial t}\right)^2 + \left(\frac{\partial w}{\partial t}\right)^2\right] \\ & + I_d\left[\left(\frac{\partial \beta_x}{\partial t}\right)^2 + \left(\frac{\partial \beta_y}{\partial t}\right)^2\right] - 2\Omega I_P\beta_x\frac{\partial \beta_y}{\partial t} + I_P\left(\frac{\partial \beta_z}{\partial t}\right)^2 \\ & + 2\Omega I_P\frac{\partial \beta_z}{\partial t} + \Omega^2 I_P + \Omega^2 I_d\left({\beta_x}^2 + {\beta_y}^2\right)dx \end{aligned} \tag{32}$$

where the $\left[I_d\left(\frac{\partial \beta_x}{\partial t}\right)^2 + \left(\frac{\partial \beta_y}{\partial t}\right)^2\right]$ represents the rotary inertia of flexional motion, the term $I_P\left(\frac{\partial \beta_z}{\partial t}\right)^2$ represents the rotary inertia of torsional motion and the term $I_m\left(\left(\frac{\partial u}{\partial t}\right)^2 + \left(\frac{\partial v}{\partial t}\right)^2 + \left(\frac{\partial w}{\partial t}\right)^2\right)$ represents the inertia of the translational motion. The term $\Omega^2 I_d\left({\beta_x}^2 + {\beta_y}^2\right)$ denotes the centrifugal stiffening effect as well as the term $2\Omega I_P\beta_x\frac{\partial \beta_y}{\partial t}$ represents the gyroscopic effect; the two last effects it will be neglected in the further analysis.where I_m, I_d and I_p are the mass per unit length of the shaft, the diametral mass of inertia and the polar mass of inertia of the cross-section of the beam, respectively. The constants I_m, I_d and I_p are expressed in Appendix A.1.

3. Governing equations and boundary conditions

The equations of motion of free vibration of composite beams are determined by means of Hamilton's principle.

$$\int_{t_0}^{t_1}(\delta T - \delta U)dt = 0 \tag{33}$$

where δT and δU are respectively the variationof kinetic and strain energies of the system. δ is the symbol of variation. In addition, t_0 and t_1 represents the time of Hamilton's action.

After the Integration by parts, then collecting the quantities δu, δv, δw, $\delta\beta_x$, $\delta\beta_y$ and $\delta\beta_z$, the following equations of motion of free vibration of a VSCL beam are obtained:

$$\begin{aligned}
&\delta u: \ I_m\frac{\partial^2 u}{\partial t^2} - \frac{\partial}{\partial x}\left[A_{11}\frac{\partial u}{\partial x} + k_s B_{16}\frac{\partial \beta_z}{\partial x}\right] = 0\\
&\delta v: I_m\frac{\partial^2 v}{\partial t^2} - k_s\frac{\partial}{\partial x}\left[(A_{55}+A_{66})\left(\frac{\partial v}{\partial x} - \beta_y\right) - \frac{1}{2}B_{16}\frac{\partial \beta_x}{\partial x}\right] = 0\\
&\delta w: I_m\frac{\partial^2 w}{\partial t^2} - k_s\frac{\partial}{\partial x}\left[(A_{55}+A_{66})\left(\frac{\partial w}{\partial x} + \beta_x\right) - \frac{1}{2}B_{16}\frac{\partial \beta_y}{\partial x}\right] = 0\\
&\delta\beta_x: I_d\frac{\partial^2 \beta_x}{\partial t^2} + I_p\Omega\frac{\partial \beta_y}{\partial t} - \frac{\partial}{\partial x}\left[\frac{1}{2}k_s B_{16}\left(\beta_y - \frac{\partial v}{\partial x}\right) + D_{11}\frac{\partial \beta_x}{\partial x}\right]\\
&\quad + \left[k_s(A_{55}+A_{66})\left(\frac{\partial w}{\partial x} + \beta_x\right) - \frac{1}{2}k_s B_{16}\frac{\partial \beta_y}{\partial x}\right] = 0\\
&\delta\beta_y: I_d\frac{\partial^2 \beta_y}{\partial t^2} - I_p\Omega\frac{\partial \beta_x}{\partial t} + \frac{\partial}{\partial x}\left[\frac{1}{2}k_s B_{16}\left(\beta_x + \frac{\partial w}{\partial x}\right) - D_{11}\frac{\partial \beta_y}{\partial x}\right]\\
&\quad + \left[k_s A_{66}\left(\beta_y - \frac{\partial v}{\partial x}\right) + \frac{1}{2}k_s B_{16}\frac{\partial \beta_x}{\partial x} - k_s A_{55}\left(\frac{\partial v}{\partial x} - \beta_y\right)\right] = 0\\
&\delta\beta_z: I_p\frac{\partial^2 \beta_z}{\partial t^2} - I_p\Omega\frac{\partial \beta_x}{\partial t} - k_s\frac{\partial}{\partial x}\left[\mathrm{B}_{16}\frac{\partial u}{\partial x} + D_{66}\frac{\partial \beta_z}{\partial x}\right] = 0
\end{aligned} \tag{34}$$

$\forall\ \delta u,\ \delta v,\ \delta w,\ \delta\beta_x,\ \delta\beta_y$ and $\delta\beta_z$

The associated boundary conditions can be assigned at both ends of the beam, taken from the conjugate sets: kinematic and natural, illustrated in Table 1.

Table 1. Kinematic and natural boundary conditions (BC).

	Kinematic BC	Natural BC
(1)	$u(x,t)=0$	$A_{11}\frac{\partial u}{\partial x} + k_s B_{16}\frac{\partial \beta_z}{\partial x} = 0$
(2)	$v(x,t)=0$	$(A_{55}+A_{66})\left(\frac{\partial v}{\partial x} - \beta_y\right) - \frac{1}{2}B_{16}\frac{\partial \beta_x}{\partial x} = 0$
(3)	$w(x,t)=0$	$(A_{55}+A_{66})\left(\frac{\partial w}{\partial x} + \beta_x\right) - \frac{1}{2}B_{16}\frac{\partial \beta_y}{\partial x} = 0$
(4)	$\beta_x(x,t)=0$	$\frac{1}{2}k_s B_{16}\left(\beta_y - \frac{\partial v}{\partial x}\right) + D_{11}\frac{\partial \beta_x}{\partial x} = 0$
(5)	$\beta_y(x,t)=0$	$\frac{1}{2}k_s B_{16}\left(\beta_x + \frac{\partial w}{\partial x}\right) - D_{11}\frac{\partial \beta_y}{\partial x} = 0$
(6)	$\beta_z(x,t)$=0	$B_{16}\frac{\partial u}{\partial x} + D_{66}\frac{\partial \beta_z}{\partial x} = 0$

4. Isogeometric approximation

In this section, we give a brief overview on the main features of the isogeometric approach. The principle idea of the isogeometric analysis IGA is to use functions from computer-aided design CAD like B-Splines to represent the geometry and to construct an approximate numerical solution in the fashion of a finite element discretization. This approach is useful because it merges design and analysis into one model.

4.1. Knot vector

A knot vector Ξ in one dimension in the parametric domain is a set of non-decreasing real values ξ_i, called knots

$$\Xi = [\xi_1, \xi_2, \xi_3, \ldots, \xi_i, \ldots, \xi_k] \tag{35}$$

with$\xi_1 \le \xi_2 \le \ldots \le \xi_i \le \ldots \ \le \xi_k$. where ξ_i is the ith knot and i is the knot index, $i = 1, 2, \ldots, k$. The number of knots verifies $k = n + p + 1$, in which$n$ is the number of basis functions, which comprise the B-spline, it's also the number of control points and p is the degree of the basis function.

Note, if a knot vector is composed of knots equally-spaced in the parametric space is said to be uniform and otherwise, it is called a non-uniform knot vector. If the knot vector is chosen equal to a set of following integers, we refer to natural B-spline. More than one knot can be located at the same coordinate in the parametric space. These are referred to as repeated knots. Moreover, if the first and last knots have the multiplicity equals to $p+1$, the knot vector is said to be open or clamped. This property is very important in applying the boundary conditions in IGA.

4.2. B-spline basis function

The B-spline functions are defined recursively on the vector of knots using Cox-de-Boor recursive formula, starting with $p = 0$ as

$$N_{i,0}(\xi) = \begin{cases} 1 \ \ if \ \ \xi \le \xi < \xi_{i+1} \\ 0 \ \ otherwise, \end{cases} \tag{36}$$

and

For $p \ge 1$,

$$N_{i,p}(\xi) = \frac{\xi - \xi_i}{\xi_{i+p} - \xi_i}N_{n,p-1}(\xi) + \frac{\xi_{i+p+1} - \xi}{\xi_{i+p+1} - \xi_{i+1}}N_{i+1,p-1}(\xi) \tag{37}$$

where ξ is the parametric coordinate.

Note that, for $p = 0$ and 1, the basic functions are the same as for standard linear finite element functions.

The functions defined in Eqs. (36) and (37) fulfill the necessary conditions for basic functions, also besides the properties of continuity there are other properties such as:

- the B-spline functions is not negative

$$\mathrm{N}_{i,p}(\xi) \ge 0 \ \forall \ \xi \in [\xi_1, \xi_i]; \ \ i = 1\ldots n \tag{38}$$

The non-negativity of the functions affects the mass matrix property of the isogeometric element i.e. all of the coefficients of a mass matrix are positive valued terms.

- Partition of unity of the B-spline functions,

$$\sum_{\mathrm{i}=1}^{n}\mathrm{N}_{i,p}(\xi) = 1 \ \forall \ \xi \ \in [\xi_1, \xi_i] \tag{39}$$

For an open knot vector, the sum of the functions equal one at a this knot.

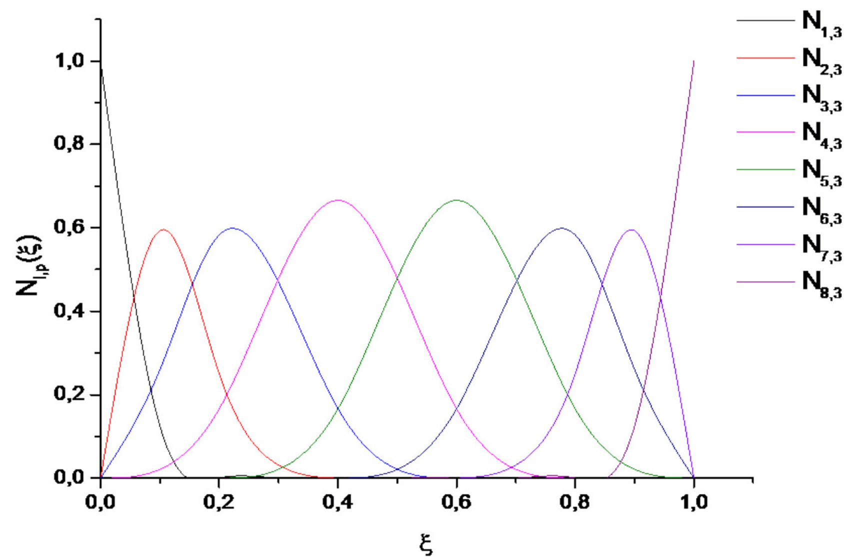

Figure 6. The cubic basis functions for an open knot vector $\Xi = [0,0,0,0.2,0.4,0.6,0.8,1,1,1,1]$.

Table 2. The cubic basis functions for an open knot vector $\Xi = .[0,0,0,0,0.2,0.4,0.6,0.8,1,1,1,1]$

		$[0,0.2]$	$[0.2,0.4]$	$[0.4,0.6]$	$[0.6,0.8]$	$[0.8,1]$
Basic functions	$N_{1,3}$	$-(5\xi-1)^3$	0	0	0	0
	$N_{2,3}$	$\frac{5\xi(175\xi^2-90\xi+12)}{4}$	$-\frac{(5\xi-2)^3}{4}$	0	0	0
	$N_{3,3}$	$-\frac{25\xi^2(55\xi-18)}{12}$	$\frac{875\xi^3}{12}-75\xi^2+\frac{45\xi}{2}-\frac{3}{2}$	$-\frac{(5\xi-3)^3}{6}$	0	0
	$N_{4,3}$	$\frac{125\xi^3}{6}$	$50\xi^2-\frac{125\xi^3}{2}-10\xi+\frac{2}{3}$	$\frac{125\xi^3}{2}-100\xi^2+50\xi-\frac{22}{3}$	$-\frac{(5\xi-4)^3}{6}$	0
	$N_{5,3}$	0	$\frac{(5\xi-1)^3}{6}$	$\frac{175\xi^2}{2}-\frac{125\xi^3}{2}-\frac{75\xi}{2}+\frac{31}{6}$	$\frac{125\xi^3}{2}-\frac{275\xi^2}{2}+\frac{195\xi}{2}-\frac{131}{6}$	$-\frac{125(\xi-1)^3}{6}$
	$N_{6,3}$	0	0	$\frac{(5\xi-2)^3}{6}$	$\frac{575\xi^2}{4}-\frac{875\xi^3}{12}-\frac{365\xi}{4}+\frac{227}{12}$	$\frac{25(\xi-1)^2(55\xi-37)}{12}$
	$N_{7,3}$	0	0	0	$\frac{(5\xi-3)^3}{4}$	$-\frac{5(\xi-1)(175\xi^2-260\xi+97)}{4}$
	$N_{8,3}$	0	0	0	0	$(5\xi-4)^3$

- The support of each $N_{i,p}(\xi)$ is compact and contained in the interval $[\xi_i, \xi_{i+p+1}]$.
- The basis functions $N_{i,p}(\xi)$, $i = 1, \ldots, n$ are piecewise polynomials of degree$p$.

In addition, if the internal knots are not repeated, the B-spline functions are C^{p-1} continuous. However, if a knot has the multiplicity k, the functions are C^{p-k} continuous at the particular knot. This means that basic function may have interpolatory property at the interior knot if the knot has the multiplicity$p$.

An example of B-Spline basis functions with $p = 3$ for an open knot vector $\Xi = [0,0,0,0,0.2,0.4,0.6,0.8,1,1,1,1]$ can be found in Figure 6. The group basis functions represented in previous figure are given in the following Table 2.

According to the B-spline basis functions $N_{i,p}(\xi)$ of order p, a B-spline curve $S(\xi)$ can be defined as

$$S(\xi) = \sum_{i=1}^{n} N_{i,p}(\xi) B_i \tag{40}$$

where n is the number of control points, B_i is the control point coordinate and $N_{i,p}(\xi)$ are the B-spline basis functions.

5. Isogeometric analysis formulation

In the IGA, the domain consists of couple of patches and each patch plays the role of sub domain or macro-element with in which element type and material models are assumed to be uniform. The patch is defined over a parametric domain, which is specified by a knot vector defining the basis function, while the physical domain is formulated by control points associated with these functions, as shown in Figure 7. The intervals defined by a knot vector are called the IGA elements. Similar to the FEM, an IGA element is specified by a set of control points (nodes) on which boundary conditions are applied and corresponding basis functions called B-spline function.

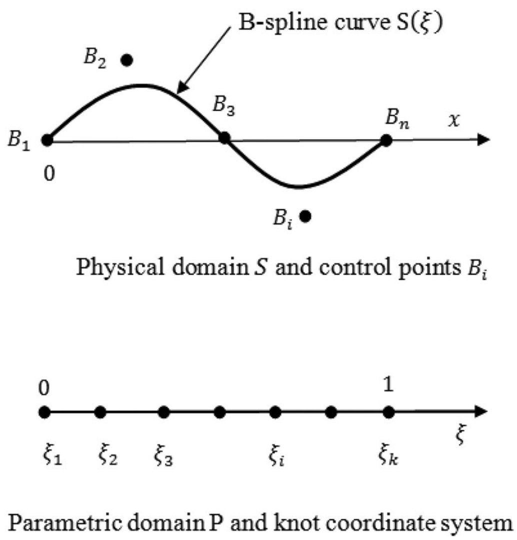

Figure 7. Physical and parametric domains.

A new beam IGA element with six degrees of freedom per control point is developed, three displacements u and v and w and three slopes β_x, β_y and β_z about x, y and z-axes, respectively. In IGA formulation, knot spans between not-repeating knots in the knot vectors become the integration ranges for the calculation of different matrices and one-knot span is defined as an isogeometric element.

The B-spline basis function $N_{i,p}$ are applied for both the parameterization of the geometry and the approximation of the displacement vector.

Following the isoparametric concept, the mapping from the parametric domain P to the physical domain S in the IGA, is expressed as

$$x(\xi) = \sum_{i=1}^{n} N_{\mathrm{i},p}(\xi) B_i \tag{41}$$

Similar to the geometry discretization, the displacements u, v, w and rotations β_x, β_y and β_z are approximated as

$$\begin{aligned}
u &= \sum_{i=1}^{n} q_{u_i}(t).N_{ui,p}(\xi) = [N_u]\{q_u\} \\
v &= \sum_{i=1}^{n} q_{v_i}(t).N_{vi,p}(\xi) = [N_v]\{q_v\} \\
w &= \sum_{i=1}^{n} q_{w_i}(t).N_{wi,p}(\xi) = [N_w]\{q_w\} \\
\beta_x &= \sum_{i=1}^{n} q_{\beta_x i}(t).N_{\beta_x i,p}(\xi) = [N_{\beta_x}]\{q_{\beta_x}\} \\
\beta_y &= \sum_{i=1}^{n} q_{\beta_y i}(t).N_{\beta_y i,p}(\xi) = [N_{\beta_y}]\{q_{\beta_y}\} \\
\beta_z &= \sum_{i=1}^{n} q_{\beta_z i}(t).N_{\beta_z i,p}(\xi) = [N_{\beta_z}]\{q_{\beta_z}\}
\end{aligned} \tag{42}$$

The displacement vector may be written in matrix form as follows.

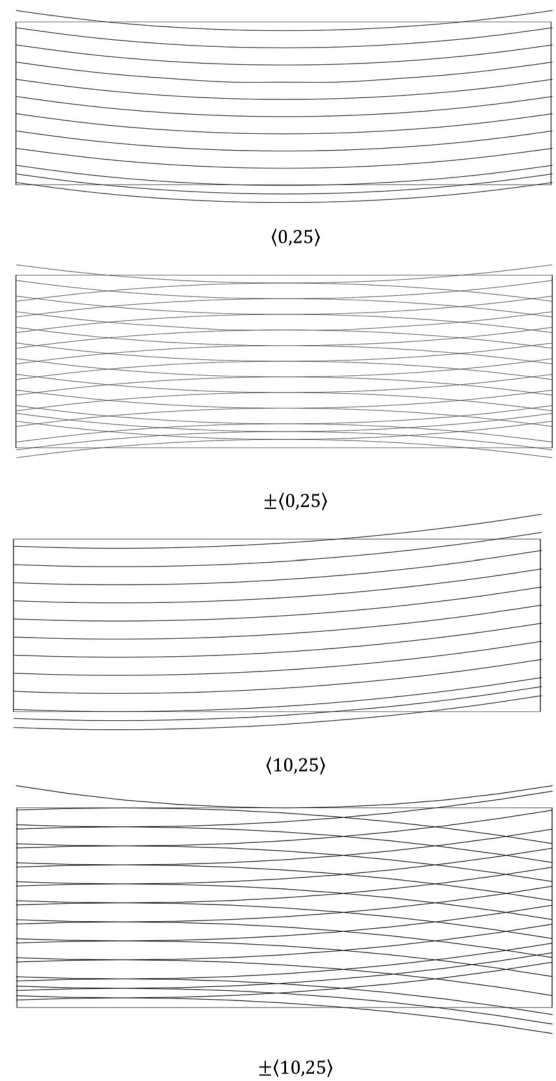

Figure 8. The configuration of VSCL beam with parabolic fiber.

$$\begin{Bmatrix} u \\ v \\ w \\ \beta x \\ \beta y \\ \beta_z \end{Bmatrix} = [N]\{q\} \tag{43}$$

where $[N]$ is the matrix consisting of basis B-spline functions, given by

$$[N] = \begin{bmatrix} [N_u] & 0 & 0 & 0 & 0 & 0 \\ 0 & [N_v] & 0 & 0 & 0 & 0 \\ 0 & 0 & [N_w] & 0 & 0 & 0 \\ 0 & 0 & 0 & [N_{\beta_x}] & 0 & 0 \\ 0 & 0 & 0 & 0 & [N_{\beta_y}] & 0 \\ 0 & 0 & 0 & 0 & 0 & [N_{\beta_z}] \end{bmatrix} \tag{44}$$

and $\{q\}$ is the vector of generalized displacements at control points, given by

Table 3. The mechanical properties of composite materials.

Material	E_1(GPA)	E_2(GPA)	G_{12}(GPA)	G_{23}(GPA)	ν_{12}	$\rho(Kg/m^3)$
Carbon-epoxy	130.0	10.0	7.0	7.0	0.25	1500

Table 4. Convergence of the first three natural frequencies of a VSCL beam $[45/45/45/\langle 0,25\rangle/\langle 0,25\rangle]$ with the boundary conditions: S-S using h-refinement.

				Mode		
p	*Nel*	*n*	dof	1	2	3
2	4	6	31	367.1206	1290.8045	2718.1654
	6	8	43	366.0682	1257.1797	2434.5214
	8	10	55	365.8990	1252.7238	2395.7861
	10	12	67	365.8540	1251.6607	2387.4081
	12	14	79	365.8381	1251.3064	2384.8019
	14	16	91	365.8313	1251.1612	2383.7803
	16	18	103	365.8280	1251.0928	2383.3127
Converged solution				365.8280	1251.0928	2383.3127

Table 5. Convergence of the first three natural frequencies of a VSCL beam $[45/45/45/\langle 0,25\rangle/\langle 0,25\rangle]$ with the boundary conditions: S-S using p-refinement.

					Mode	
Nel	*p*	*n*	dof	1	2	3
4	3	10	55	365.8350	1251.5874	2387.8708
	4	14	79	365.8235	1251.0042	2382.9412
	5	18	103	365.8235	1250.9994	2382.7012
	6	22	127	365.8235	1250.9994	2382.6995
Converged IGA solution				365.8235	1250.9994	2382.6995

$$\{q\} = \left\{ \begin{array}{c} \{q_u\} \\ \{q_v\} \\ \{q_w\} \\ \{q_{\beta_x}\} \\ \{q_{\beta_y}\} \\ \{q_{\beta_z}\} \end{array} \right\} \tag{45}$$

Using the Galerkin method, a weak formulation of the free vibration of the VSCL beam is obtained as:

$$\begin{aligned}
&\sum_{e=1}^{Nel} \int_{k_e}^{k_{e+1}} [\delta u I_m \ddot{u} + \delta v I_m \ddot{v} + \delta w I_m \ddot{w} + \delta\beta_x I_d \ddot{\beta}_x \\
&+ \delta\beta_y I_d \ddot{\beta}_y + \delta\beta_z I_p \ddot{\beta}_z + \delta\beta_x I_p \dot{\beta}_y] \\
&- \delta\beta_y I_p \dot{\beta}_x + \frac{1}{J}\frac{\partial \delta u}{\partial \xi}\left[k_s A_{16}\frac{1}{J}\frac{\partial \beta_z}{\partial \xi} + A_{11}\frac{1}{J}\frac{\partial u}{\partial \xi}\right] \\
&+ \ k_s \frac{1}{J}\frac{\partial \delta v}{\partial \xi}\left[-A_{16}\frac{1}{J}\frac{\partial \beta_x}{\partial \xi} + (A_{55}+A_{66})\left(\frac{1}{J}\frac{\partial v}{\partial \xi} - \beta_y\right)\right] \\
&+ k_s \frac{1}{J}\frac{\partial \delta w}{\partial \xi}\left[-A_{16}\frac{1}{J}\frac{\partial \beta_y}{\partial x} + (A_{55}+A_{66})\left(\beta_x + \frac{1}{J}\frac{\partial w}{\partial \xi}\right)\right] \\
&+ \frac{1}{J}\frac{\partial \delta\beta_x}{\partial \xi}\left[B_{11}\frac{1}{J}\frac{\partial \beta_x}{\partial \xi} + k_s A_{16}\left(\beta_y + \frac{1}{J}\frac{\partial v}{\partial \xi}\right)\right] \\
&+ \frac{1}{J}\frac{\partial \delta\beta_y}{\partial \xi}\left[B_{11}\frac{1}{J}\frac{\partial \beta_y}{\partial \xi} - k_s A_{16}\left(\beta_x + \frac{1}{J}\frac{\partial w}{\partial \xi}\right)\right] \\
&+ k_s \frac{1}{J}\frac{\partial \delta\beta_z}{\partial \xi}\left[B_{66}\frac{1}{J}\frac{\partial \beta_z}{\partial \xi} + A_{16}\frac{1}{J}\frac{\partial u}{\partial \xi}\right] \\
&+ k_s \ \delta\beta_x\left[-A_{16}\frac{1}{J}\frac{\partial \beta_y}{\partial \xi} + (A_{55}+A_{66})\left(\beta_x + \frac{1}{J}\frac{\partial w}{\partial \xi}\right)\right] \\
&\left[+ k_s \ \delta\beta_y\left[A_{16}\frac{1}{J}\frac{\partial \beta_x}{\partial \xi} + (A_{55}+A_{66})\left(\beta_y + \frac{1}{J}\frac{\partial v}{\partial \xi}\right)\right]\right] \det J \ d\xi = 0
\end{aligned} \tag{46}$$

where Nel is the number of isogeometric elements, $[k_e, \ k_{e+1}]$ is knot interval for integration and J is Jacobian of transformation between x and ξ.

Substituting Eq. (42) into Eq. (46), lead to linear algebraic equations of motion of free vibration of the composite beam

$$[M]\{\ddot{q}\} + [K]\{q\} = 0 \tag{47}$$

where $[M]$ represents the global mass matrix, $[K]$ global the stiffness matrix and can be written as

$$[K] = \prod_{e=1}^{Nel} [K]^e \tag{48}$$

$$[M] = \prod_{e=1}^{Nel} [M]^e \tag{49}$$

where $[M]^e$ represents the element mass matrix, $[K]^e$ element stiffness matrix, which $\prod_{e=1}^{Nel}$ is the element assembly operator. Details about the different matrices can be found in Appendix A.2 and A.3. in Eq. (47), $\{\ddot{q}\}$, and $\{q\}$ are respectively acceleration, and displacement vectors of control points.in order to use a complex modal analysis Eq. (47) is transformed into the following form

$$[A]\{\dot{X}\} + [B]\{X\} = 0 \tag{50}$$

where

$$[A] = \begin{bmatrix} [M] & 0 \\ 0 & [I] \end{bmatrix} \tag{51}$$

$$[B] = \begin{bmatrix} 0 & [K] \\ -[I] & 0 \end{bmatrix} \tag{52}$$

Table 6. Convergence of the first three natural frequencies of a VSCL beam $[45/45/45/\langle 0,25\rangle/\langle 0,25\rangle]$ with the boundary conditions: S-S using k-refinement.

				Mode		
Nel	*p*	*n*	dof	1	2	3
4	3	7	37	365.8389	1254.1290	2439.0395
	4	8	43	365.8236	1251.2033	2404.5064
	5	9	49	365.8235	1251.0333	2384.5674
	6	10	55	365.8235	1251.0008	2383.4718
	7	11	61	365.8235	1250.9998	2382.7424
	8	12	67	365.8235	1250.9994	2382.7144
	9	13	73	365.8235	1250.9994	2382.7002
	10	14	79	365.8235	1250.9994	2382.6997
Converged IGA solution				365.8235	1250.9994	2382.6997

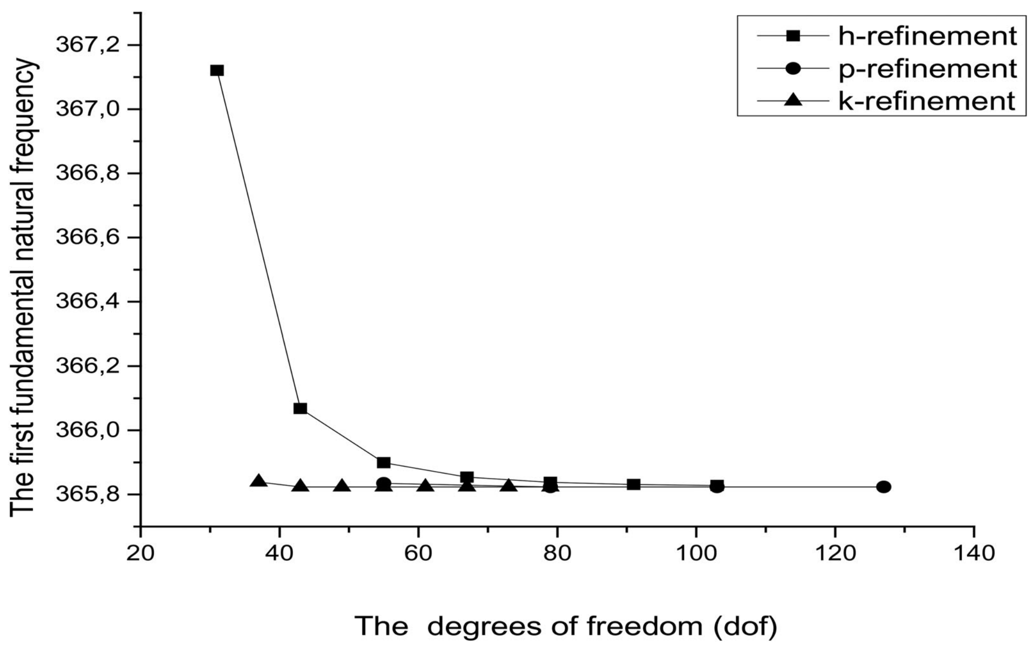

Figure 9. The first fundamental natural frequencies of the VSCL beam with increase in the degrees of freedom (dof).

$$\{X\} = \left\{ \begin{array}{c} \{\dot{q}\} \\ \{q\} \end{array} \right\} \tag{53}$$

where $[I]$ represents a unit matrix. From Eq. (50), an eigenvalue problem can be derived by assuming that $\{X\}$ is a harmonic matrix function of t expressed as

$$\{X\} = \{\overline{X}\}e^{\overline{\varpi}t} \tag{54}$$

where $\overline{\varpi}$ is the complex eigenvalue and $\{\overline{X}\}$ is the complex mode shape.

Substituting Eq. (54) into Eq. (50) yields:

$$\left[\overline{\varpi}[A] + [B]\right]\{\overline{X}\} = 0 \tag{55}$$

6. Numerical results and discussion

Several examples of the variable stiffness composite beam vibration problem are given to demonstrate the applicability of the present model and the efficient of new generation of materials used in this study. We are mainly interested in the effects of the parabolic fiber orientation, laminate stacking sequence, mechanical properties and length to mean diameter ratio, modulus of elasticity ratio and boundary conditions on the natural frequencies of the composite beam. The symbol $\langle T_0, T_1\rangle$ is the single layer containing an orientation of the parabolic fiber. The different cases of orientation angles with parabolic fiber used in this study are shown in Figure 8.

Table 3 shows the mechanical properties of the three composites materials used in the simulations: boron-epoxy, graphite-epoxy and carbon-epoxy.

6.1. Convergence study

In this section, Solution accuracy and convergence studies of the present formulation are carried out. Vibration study of variable stiffness composite beam is considered here. The material used in this section is the carbon epoxy with a simply-supported boundary conditions. The material properties are listed in Table 3, and the geometric parameters are: length, 1 m; mean radius, 0.05 m; total thickness, 4 mm. The laminate consisted of five layers oriented as follows: $[45, 45, 45, \langle 0, 25\rangle, \langle 0, 25\rangle]$.

For these purposes, three refinement schemes such as h-, p- and k-refinements are employed. We begin with quadratic basis functions ($p = 2$) and four isogeometric elements in the longitudinal direction. For the h-

Table 7. Comparison of the first three natural frequencies of a composite constant beam with the boundary conditions: S-S.

			Mode		
θ		dof	1	2	3
(45°/0°/45°/45°)	ESLT [11]		326.0000	1159.0000	2258.0000
	Present	79	325.6742	1158.3889	2256.5331
(45°/45°/0°/45°)	ESLT [11]		329.0000	1170.0000	2275.0000
	Present	79	329.5376	1169.5731	2273.3345
(45°/45°/45°/0°)	LBT [5]		319.8370	1188.5060	2422.7820
	EMBT Modifié [6]		319.5650	1185.0380	2409.6890
	ESLT [11]		333.000	1181.000	2292.000
	Present	79	333.4812	1180.9004	2290.2011

Table 8. Comparison of the first three natural frequencies of a symmetric cross-ply beam with the boundary conditions: S-S.

			Mode		
θ		dof	1	2	3
(0°/90°/90°/0°)	LBT [5]		338.9250	1071.7920	1896.808
	EMBT Modifié [6]		338.7870	1070.5390	1893.0510
	Present	79	339.4441	1071.8671	1894.5317
(90°/0°/0°/90°)	LBT [5]		338.5480	1070.3290	1893.4070
	EMBT Modifié [6]		338.5070	1069.9730	1892.4190
	Present	79	339.1639	1071.3014	1893.9013

Table 9. Comparison of the first three natural frequencies of anti-symmetric cross-ply beam with the boundary conditions: S-S.

			Mode		
θ		dof	1	2	3
(90°/0°/90°/0°)	LBT [5]		342.7750	1082.5440	1913.9620
	EMBT Modifié [6]		342.1120	1077.2280	1900.4870
	Present	79	342.7730	1078.5481	1901.9474
(0°/90°/0°/90°)	LBT [5]		334.6300	1059.2750	1875.5370
	EMBT Modifié [6]		335.1100	1063.0590	1884.6710
	Present	79	335.7635	1064.3952	1886.1729

Table 10. The first three natural frequencies of anti-symmetric and symmetric two, three and four layers VSCL beam with fiber orientation $[\pm\langle T_0, T_1\rangle]$, $T_0 = 0^\circ$ and the boundary condition: S-S.

		T_1										
Lay-up	Mode	−25	−20	−15	−10	−5	0	5	10	15	20	25
$[\pm\langle T_0, T_1\rangle]$	1	447.4074	444.2572	439.4613	434.0532	429.6013	427.8445	429.6013	434.0532	439.4613	444.2572	447.4074
	2	1309.7670	1296.1181	1275.9632	1253.0591	1233.9255	1226.3008	1233.9255	1253.0591	1275.9632	1296.1181	1309.7670
	3	2272.3989	2219.8383	2163.3070	2109.1882	2068.1398	2052.4955	2068.1398	2109.1882	2163.3070	2219.8383	2272.3989
$\begin{bmatrix} +\langle T_0, T_1\rangle, -\langle T_0, T_1\rangle \\ , +\langle T_0, T_1\rangle \end{bmatrix}$	1	445.2067	442.6103	438.3722	433.4892	429.4430	427.8445	429.4430	443.4892	438.4892	442.6103	445.2067
	2	1301.7677	1289.9850	1271.8010	1250.853	1233.2943	1226.3008	1233.2943	1250.8503	1271.8010	1289.9850	1301.7677
	3	2261.7544	2211.5364	2157.5620	2106.0861	2067.2430	2052.4955	2067.2430	2106.0861	2157.5620	2211.5364	2261.7544
$[\pm\langle T_0, T_1\rangle]_2$	1	447.4312	444.2750	439.4731	434.0594	429.6031	427.8445	429.6031	434.0594	439.4731	444.2750	447.4312
	2	1309.8535	1296.1845	1276.0084	1253.0831	1233.9324	1226.3008	1233.9324	1253.0831	1276.0084	1296.1845	1309.8535
	3	2272.5138	2219.9281	2163.3693	2109.2219	2068.1496	2052.4955	2068.1496	2109.2219	2163.3693	2219.9281	2272.5138
$[\pm\langle T_0, T_1\rangle]_s$	1	447.4392	444.2810	439.4770	434.0614	429.6036	427.8445	429.6036	429.0614	439.4770	444.2810	447.4392
	2	1309.8824	1296.2067	1276.0235	1253.0911	1233.9347	1226.3008	1233.9347	1253.0911	1276.0235	1296.2067	1309.8824
	3	2272.5521	2219.9580	2163.3900	2109.2331	2068.1528	2052.4955	2068.1528	2109.2331	2163.3900	2219.9580	2272.5521

refinement test, the number of elements is increased up to 16 elements, gradually. For the p-refinement test, four isogeometric elements are used and the orders of basis function is increased up to $p\ = 6$. The same strategy is adopted for thek-refinement, however, the orders of basis function is increased up to $p\ = 10$. It should be noted that the knots located between adjacent two elements must be inserted in such a way as to ensure C^0 and C^{p-1} continuity for p- and k-refinements, respectively.

Results for the three lowest frequencies of h-, p- and k-refinements are illustrated respectively in Tables 4–6.

Good convergence and accuracy of the first three frequencies parameters are obtained by increasing the number of elements or the degree of basic functions.

Sixteen isogeometrics elements with quadratic basis functions are used in the h-refinement. In this case, the number of control points is 18 and the corresponding number of system degrees of freedom (dof) is 103. As shown in Table 4, the first

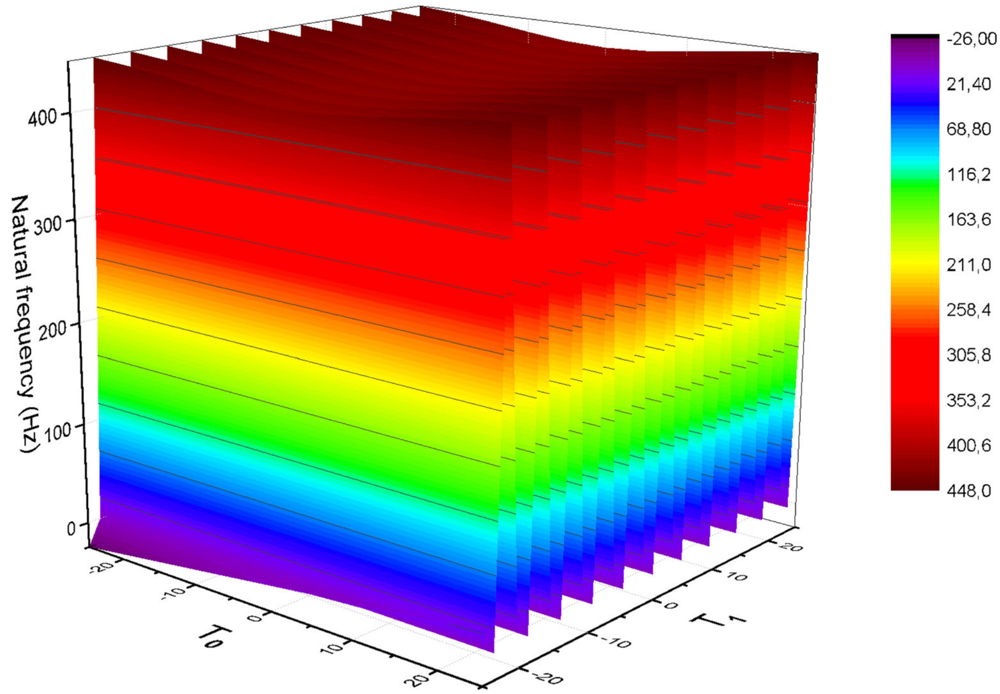

Figure 10. Variation of the first fundamental natural frequency of anti-symmetric two layers VSCL beam $[\pm\langle T_0, T_1\rangle]$, with $T_0 = 0$ and the boundary conditions: S-S.

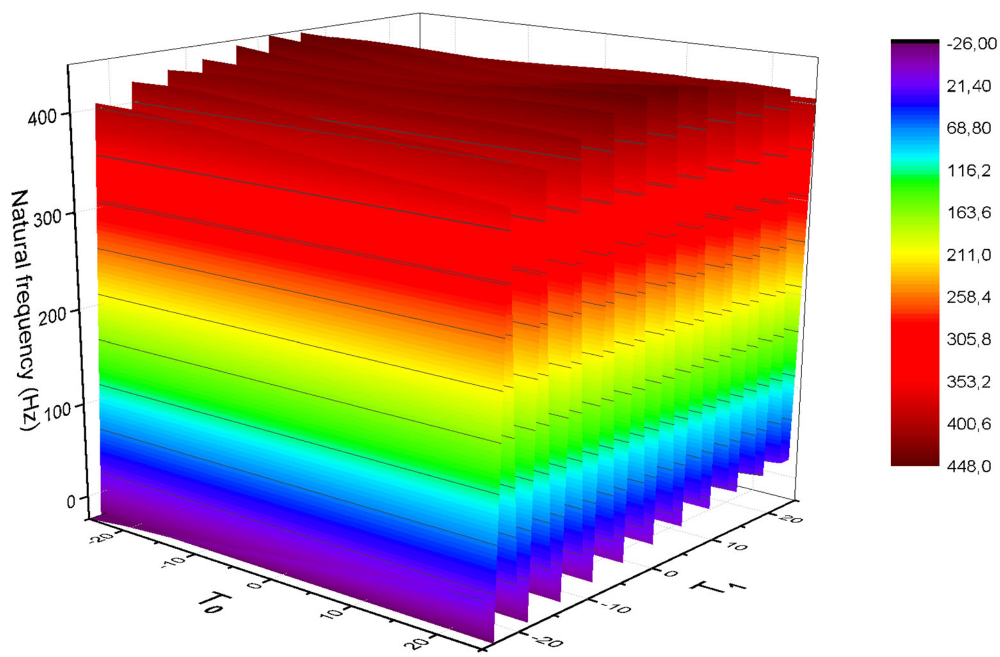

Figure 11. Variation of the first fundamental natural frequency of anti-symmetric two layers VSCL beam $[\pm\langle T_0, T_1\rangle]$, with T_0 variable and the boundary conditions: S-S.

three frequencies are computed with maximum error of 0.0194%.

In the case of the *p*-refinement, the degree of basic functions is increased to $p = 6$ without changing the number of elements ($Nel = 4$), the number of control points is 22 and the corresponding number of system dof is 127. As shown in Table 5, the first three frequencies are computed with maximum error of 0.0001%.

The same number of elements is used in numerical test given by the *k*-refinement, while*p* is increased to 10. The number of control points and the corresponding total number of system dof used in the computation is respectively 14 and 79, the maximum error is equal to 0.000021%

Tables 4–6 clearly show that the *h*-refinement produces a slow convergence to the converged values (365.8235, 1250.9994, 2382.6997, see Tables 5 and 6) compared to the other p- and k-refinements. The *p*-refinement shows a better convergence rate than the *k*-refinement if the same number of element and degree of basis functions are employed in numerical test, for example for $p = 6$ the maximum error

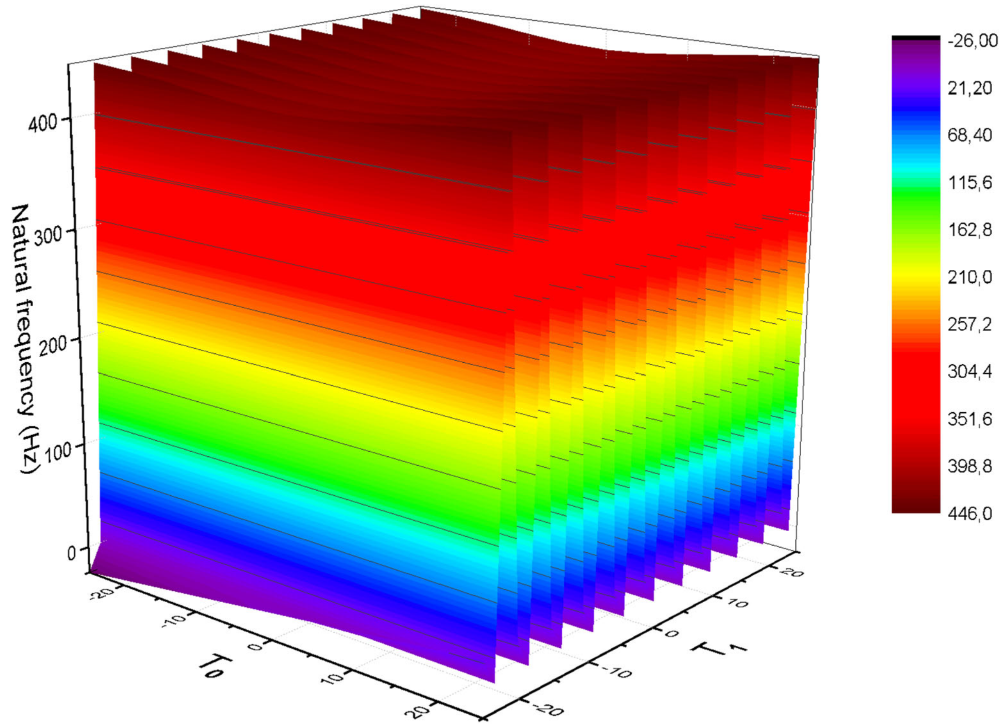

Figure 12. Variation of the first fundamental natural frequency of symmetric three layers VSCL beam $[+\langle T_0, T_1\rangle, -\langle T_0, T_1\rangle, +\langle T_0, T_1\rangle]$, with $T_0 = 0$ and the boundary conditions: S-S.

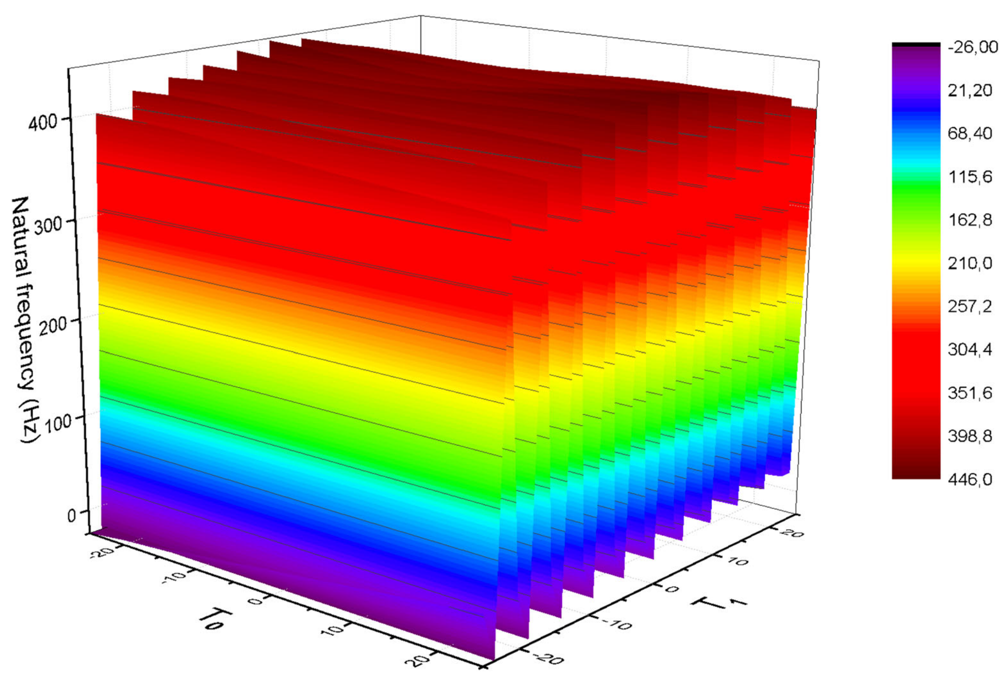

Figure 13. Variation of the first fundamental natural frequency of symmetric three layers VSCL beam $[+\langle T_0, T_1\rangle, -\langle T_0, T_1\rangle, +\langle T_0, T_1\rangle]$, with T_0 variable and the boundary conditions: S-S.

is equal to 0.0324% for k-refinement and only 0.0001% for *p*-refinement. The converged values are reached by using 22 control points and 127 dof (*p*-refinement).

If on the other hand we increase the degree of the functions to $p = 10$ for the k-refinement, the error will decrease until 0.000021% and the converged values are reached by using only 14 control points and 79 dof despite the use of about 38% fewer system degrees of freedom than the *p*-refinement solutions.

From this convergence study, it can be seen that the total degree of freedom due to *p*-refinement is greater than those of *k*-refinement for the same accuracy. This discussions it's clearly show as in Figure 9. The *k*-refinement is more advantageous than the *h*- and *p*-refinements in computation,

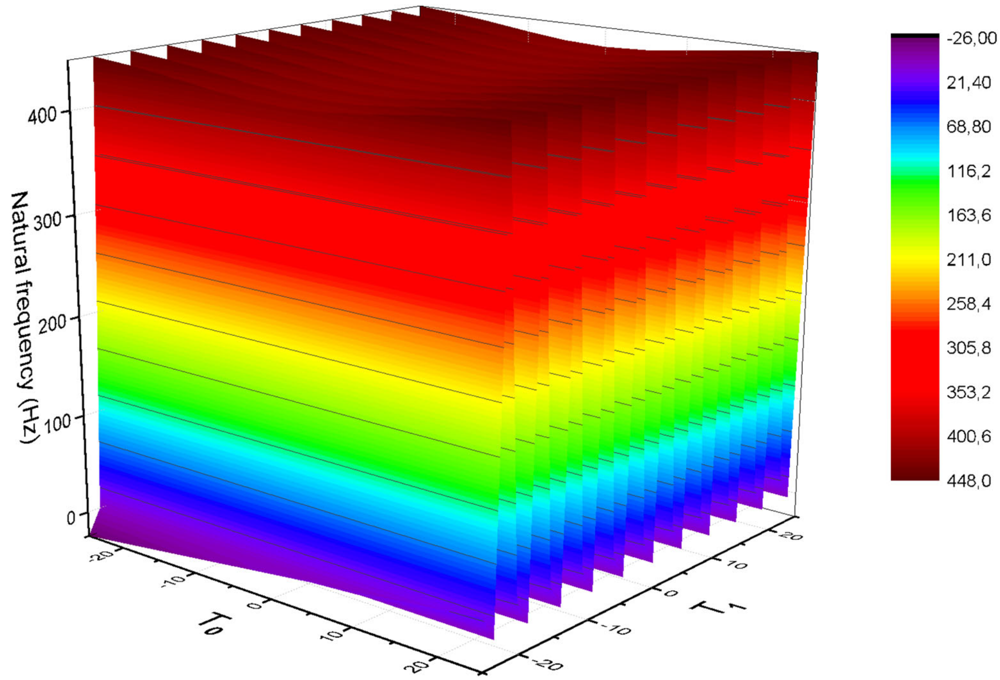

Figure 14. Variation of the first fundamental natural frequency of anti-symmetric four layers VSCL beam $[\pm\langle T_0, T_1\rangle]_2$, with $T_0 = 0$ and the boundary conditions: S-S.

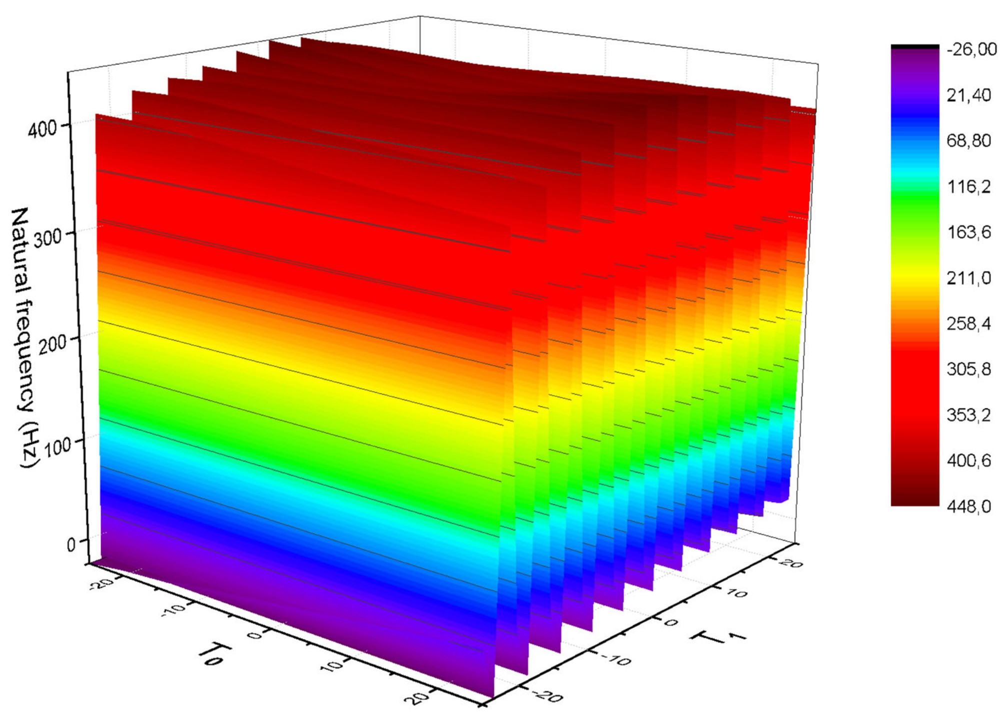

Figure 15. Variation of the first fundamental natural frequency of symmetric four layers VSCL beam $[\pm\langle T_0, T_1\rangle]_2$, with T_0 variable and the boundary conditions: S-S.

by consequent the k-refinement scheme with $p = 10$ and $Nel = 4$ is used in the next section.

6.2. Composite beam with constant stiffness

In the second example, a comparison study is carried out for constant stiffness composite beam, to verify results accuracy, the laminate consisted of four layers oriented as shown in Table 7, the natural frequencies obtained from present analysis agree well with that of Singh and Gupta [5] using layer wise beam theory (LBT), Gubran and Gupta [6] using Modified EMBT and Ben Arab et al. [11] using Equivalent Single Layer Theory (ESLT);

Tables 7–9 gives the results of the first three natural frequencies of composite beam in the cases of symmetric and anti-symmetric cross-ply with the number of layers equal four. The results obtained from present analysis are in good

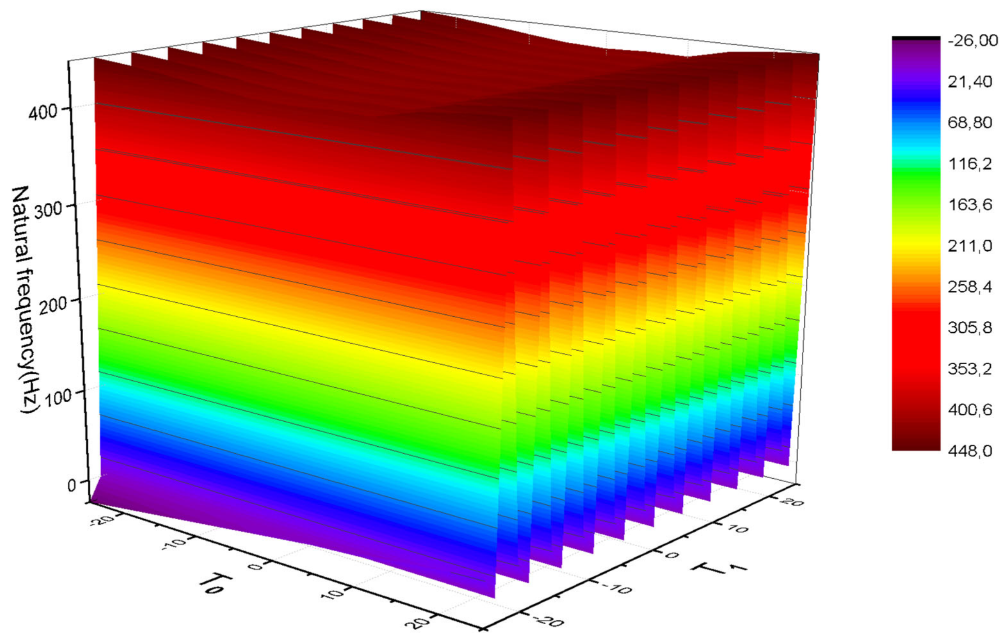

Figure 16. Variation of the first fundamental natural frequency of anti-symmetric four layers VSCL beam $[\pm\langle T_0, T_1\rangle]_s$, with $T_0 = 0$ and the boundary conditions: S-S.

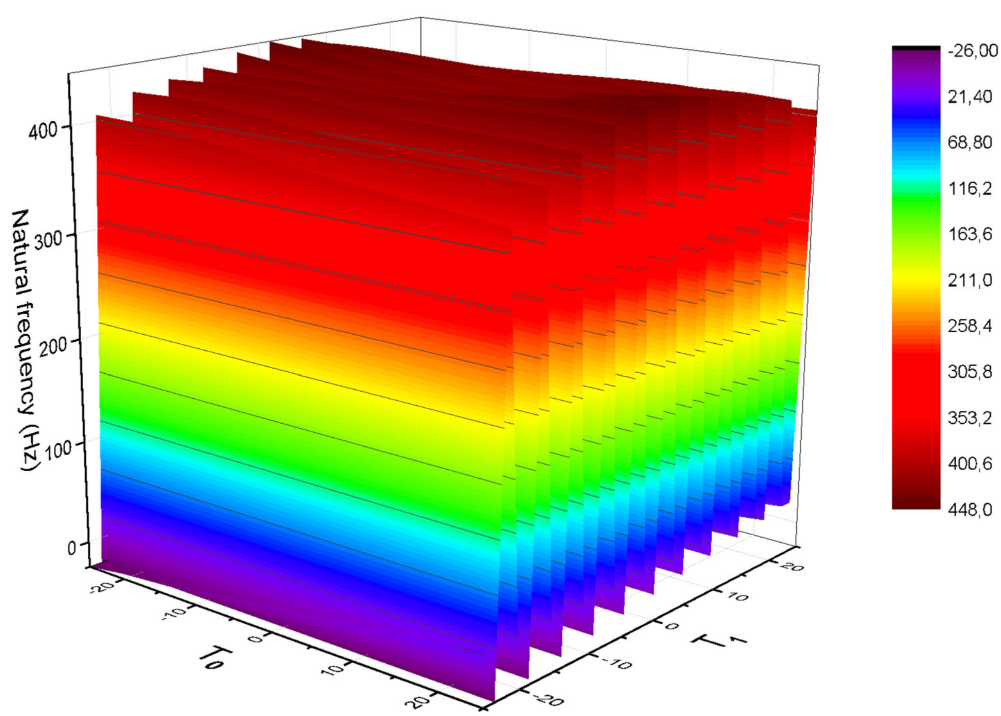

Figure 17. Variation of the first fundamental natural frequency of symmetric four layers VSCL beam $[\pm\langle T_0, T_1\rangle]_s$, with T_0 variable and the boundary conditions: S-S.

agreement with Singh and Gupta [5] using layer wise beam theory (LBT), and Gubran and Gupta [6] using Modified EMBT.

6.3. Composite beam with variable stiffness

Due to the relative lack of publications on vibrations of composite beams reinforced with parabolic fibers, this section is devoted to investigate the effect of the fibers $\langle T_0, T_1\rangle$, the physical and geometrical parameters, and the boundary conditions on the first natural frequencies of composite beam with parabolic fiber path.

The first investigation, a study is made to determine the first three natural frequencies of a variable stiffness composite beam with two, three and four symmetric and anti-symmetric layers respectively using the k-refinement scheme with $p = 10$ and $Nel\ = 4$ as shown in Table 10. The mechanical parameters of carbon-epoxy used are shown in Table 3. The study showed the effect of variation of the layers' number and the orientation of curved fibers $\langle T_0, T_1\rangle$ on the natural frequencies, in which the fiber orientation T_0 keep to 0° whereas the fiber orientation angle T_1 varies from -25° to 25° with an increment of 5°. As shown in Table 10, the first natural frequency of two, three, and four symmetric

Table 11. The first three natural frequencies of anti-symmetric and symmetric five, six and seven layers VSCL beam with the boundary conditions: S-S and $T_0 = 0$.

		T_1										
Lay-up	Mode	−25	−20	−15	−10	−5	0	5	10	15	20	25
$[45_3/\pm\langle T_0, T_1\rangle]$	1	365.8235	367.2004	368.0498	368.5259	368.7543	368.8024	368.7543	368.5259	368.0498	367.2004	365.8235
	2	1250.9994	1258.0180	1262.0305	1263.9933	1264.7608	1264.9423	1264.7608	1263.9933	1262.0305	1258.0180	1250.9994
	3	2382.6997	2386.1700	2385.9669	2383.9429	2381.8533	2380.9957	2381.8533	2383.9429	2385.9669	2386.1700	2382.6997
$\begin{bmatrix} 45_3, +\langle T_0, T_1\rangle, \\ -\langle T_0, T_1\rangle, \\ +\langle T_0, T_1\rangle \end{bmatrix}$	1	385.0196	386.4613	387.2599	387.6320	387.7655	387.7937	387.7655	387.6320	387.2599	386.4613	385.0196
	2	1289.0101	1295.5177	1298.5470	1299.3917	1299.2789	1299.1263	1299.2789	1299.3917	1298.5470	1295.5177	1289.0101
	3	2415.8125	2414.8400	2410.0890	2404.0259	2399.1078	2397.2279	2399.1078	2404.0259	2410.0890	2414.8400	2415.8125
$[45_3/\pm\langle T_0, T_1\rangle_2]$	1	398.0499	399.1262	399.5111	399.4924	399.3425	399.2666	399.3425	399.4924	399.5111	399.1262	398.0449
	2	1313.2691	1317.4637	1317.9173	1316.3416	1314.4697	1313.6691	1314.4697	1316.3416	1317.9173	1317.4637	1313.2691
	3	2432.2927	2424.9692	2413.8728	2402.2043	2393.3464	2390.0363	2393.3464	2402.2043	2413.8728	2424.9692	2432.2927
$[45_3/\pm\langle T_0, T_1\rangle_s]$	1	398.0457	399.1267	399.5115	399.4925	399.3425	399.2666	399.2425	399.5115	399.5115	399.1267	399.0457
	2	1313.2730	1317.4665	1317.9190	1316.3425	1314.4699	1313.6691	1314.4699	1316.3425	1317.9190	1317.4665	1313.2730
	3	2432.2989	2424.9738	2413.8757	2402.2057	2393.3467	2393.3467	2393.3467	2402.2057	2413.8757	2424.9738	2432.2989

Table 12. The first three natural frequencies of anti-symmetric and symmetric nine, and eleven layers VSCL beam with the boundary conditions: S-S and $T_0 = 0$.

		T_1										
Lay-up	Mode	−25	−20	−15	−10	−5	0	5	10	15	20	25
$[45_3/\pm\langle T_0, T_1\rangle_3]$	1	412.7516	413.3999	413.2409	412.6762	412.1139	411.8832	412.1139	412.6762	413.2409	413.3999	412.7516
	2	1332.3662	1333.8283	1331.1226	1326.4553	1322.2583	1320.5843	1322.2583	1326.4553	1331.1226	1333.8283	1332.3662
	3	2430.3019	2414.9697	2395.9052	2377.1176	2363.1723	2357.9939	2363.1723	2377.1176	2395.9052	2414.9697	2430.3019
$\begin{bmatrix} 45_3, (+\langle T_0, T_1\rangle, \\ -\langle T_0, T_1\rangle, \\ +\langle T_0, T_1\rangle) \end{bmatrix}_s$	1	411.8400	412.7568	412.8443	412.4856	412.0636	411.8832	412.0636	412.4856	412.8443	412.7568	411.8400
	2	1327.9977	1330.6235	1329.1157	1325.4720	1321.9956	1320.5843	1321.9956	1325.4720	1329.1157	1330.6535	1327.9977
	3	2423.6485	2410.0333	2329.7237	2375.5335	2362.7446	2357.9939	2362.7446	2375.5335	2392.7237	2410.0333	2423.6485
$[45_3/\pm\langle T0, T1\rangle_4]$	1	421.0030	421.2550	420.6134	419.5645	418.6327	418.2622	418.6327	419.5645	420.6134	421.2550	421.0030
	2	1338.8868	1338.2080	1333.0558	1325.9680	1319.9183	1317.5397	1319.9183	1325.9680	1333.0558	1338.2080	1338.8868
	3	2418.9508	2397.8693	2373.0802	2349.1099	2331.3957	2324.8166	2331.3957	2349.1099	2373.0802	2397.8693	2418.9508
$[45_3/(\pm\langle T0, T1\rangle_2)_s]$	1	421.0035	421.2554	420.6137	419.5646	418.6328	418.2622	418.6328	419.5646	420.6137	421.2554	421.0035
	2	1338.8891	1338.2097	1333.0569	1325.9685	1319.9184	1317.5397	1319.9184	1325.9685	1333.0569	1338.2097	1338.8891
	3	2418.9543	2397.8719	2373.0819	2349.1107	2331.3959	2324.8166	2331.3959	2349.1107	2373.0819	2397.8719	2418.9543

and anti-symmetric layers is increased when the value of the fiber orientation increases, in which T_1 varies from 0° to 25° by 4.373%, 3.9%, 4.378% and 4.379% respectively. Table 10 clearly show that the natural frequencies are influenced by the variation of orientation angles of the parabolic fibers and the number of the layers when the aforementioned variables becomes large.

In the next examples as shown in Figures 10–17, the same configurations of laminate of previous example (Table 10) are used, while the fiber orientation angle T_0 keep to 0°; whereas the fiber orientation angle T_1 varies from -25° to 25° in the first case, and in the second the fiber orientation angle T_0 varies from 0° to -25°; whereas the fiber orientation angle T_1 varies from -25° to 25°. The increment size is 5°.

According to the results listed in Figures 10–17, for example, it can be seen that the first natural frequency is decreased when the value of the fiber orientation angle increases, in which T_0 varies from -25° to 25° by 16.452%, 17.028%, 16.454%, 16.452% for two, three and four anti-symmetric and symmetric layers as show in Figures 11, 13, 15, and 17 and increase when T_0 keep to 0°; as show in Figures 10, 12, 14, and 16 respectively.

Figures 10–17 clearly show that when the fiber orientation angle T_0 varies from -25° to 25° produces a less stiffness to the (447.4070, 445.2065, 447.4312, 447.4392 see Table 10) compared to the other cases when the orientation angle T_0 equal to 0°.

The fiber orientation angle T_0 equals to zero is more advantageous than T_0 varies from -25° to 25° in the optimization of variable stiffness composite beam, by consequent the fiber orientation angle T_0 equals to zero is used in the next section.

The effects of stacking sequence, number of layers and angle lamination of a carbon-epoxy beam bi- simply supported with $[45^\circ/45^\circ/45^\circ/\pm\langle T0, T1\rangle]$ lay-ups on the natural frequencies are illustrated in Tables 11 and 12, in which the fiber orientation T_0 keep to 0° whereas, the fiber orientation angle T_1 varies from -25^0 to 25^0 with an increment of 5^0.

The first observation can be that, the natural frequency increases with an increment in the number of parabolic fibers angle orientations $\pm\langle T_0, T_1\rangle$ varies from 2 to 8 layers. The second observation is the effect of symmetric and anti-symmetric-layups, it can be seen that all values of natural frequency are little increase than the natural frequencies in case of symmetric-layups.

In order to show the effect of variable stiffness composite materials, a Comparison between the VSCL beam and the CSCL beam with $[45^\circ/45^\circ/45^\circ/\pm\langle T_0, T_1\rangle]$ lay-ups in which the number of the fiber parabolic orientation two, three, four, six, and eight symmetric and anti-symmetric layers respectively is presented as in Tables 13–16. The same

Table 13. Comparison between the first three natural frequencies of anti-symmetric and symmetric VSCL and CSCL beam with the boundary conditions: S-S.

Lay-up	Mode	T_1										
VSCL		$\langle 0,-25\rangle$	$\langle 0,-20\rangle$	$\langle 0,-15\rangle$	$\langle 0,-10\rangle$	$\langle 0,-5\rangle$	0	$\langle 0,5\rangle$	$\langle 0,10\rangle$	$\langle 0,15\rangle$	$\langle 0,20\rangle$	$\langle 0,25\rangle$
$[45_3, \pm\langle T_0, T_1\rangle]$	1	365.8235	367.2004	368.0498	368.5259	368.7543	368.8024	368.7543	368.5259	368.0498	367.2004	365.8235
	2	1250.9994	1258.0180	1262.0305	1263.9933	1264.7608	1264.9423	1264.7608	1263.9933	1262.0305	1258.0180	1250.9994
	3	2382.6997	2386.1700	2385.9669	2383.9429	2381.8533	2380.9957	2381.8533	2383.9429	2385.9669	1250.9994	2382.6997
CSCL		$\langle -25,-25\rangle$	$\langle -20,-20\rangle$	$\langle -15,-15\rangle$	$\langle -10,-10\rangle$	$\langle -5,-5\rangle$	0	$\langle 5,5\rangle$	$\langle 10,10\rangle$	$\langle 15,15\rangle$	$\langle 20,20\rangle$	$\langle 25,25\rangle$
$[45_3, \pm\langle T_0, T_1\rangle]$	1	336.3109	348.1662	357.1877	363.7336	367.3862	368.8024	367.5722	364.0882	357.6770	348.7524	336.9567
	2	1199.6391	1227.8775	1246.3285	1257.7607	1262.7996	1264.9423	1263.3799	1258.8788	1247.8970	1229.7936	1201.7943
	3	2342.1088	2370.8038	2382.4556	2384.6729	2381.5487	2380.9957	2382.5206	2386.5615	2385.1412	2374.1418	2345.9392
VSCL		$\langle 0,-25\rangle$	$\langle 0,-20\rangle$	$\langle 0,-15\rangle$	$\langle 0,-10\rangle$	$\langle 0,-5\rangle$	0	$\langle 0,5\rangle$	$\langle 0,10\rangle$	$\langle 0,15\rangle$	$\langle 0,20\rangle$	$\langle 0,25\rangle$
$[45_3, (+\langle T_0, T_1\rangle, -\langle T_0, T_1\rangle, +\langle T_0, T_1\rangle)]$	1	385.0196	386.4613	387.2599	387.6320	387.7655	387.7937	387.7655	387.6320	387.2599	386.4613	385.0196
	2	1289.0101	1295.5177	1298.5470	1299.3917	1299.2789	1299.1263	1299.2789	1299.3917	1298.5470	1295.5177	1289.0101
	3	2415.8125	2414.8400	2410.0890	2404.0259	2399.1078	2397.2279	2399.1078	2404.0259	2410.0890	2414.8400	2415.8125
CSCL		$\langle -25,-25\rangle$	$\langle -20,-20\rangle$	$\langle -15,-15\rangle$	$\langle -10,-10\rangle$	$\langle -5,-5\rangle$	0	$\langle 5,5\rangle$	$\langle 10,10\rangle$	$\langle 15,15\rangle$	$\langle 20,20\rangle$	$\langle 25,25\rangle$
$[45_3, (+\langle T_0, T_1\rangle, -\langle T_0, T_1\rangle, +\langle T_0, T_1\rangle)]$	1	357.5083	370.7354	380.1496	386.1526	388.3583	387.7937	384.2021	378.2939	369.4167	358.0132	343.6106
	2	1261.2655	1288.5108	1302.5337	1307.1498	1304.2353	1299.1263	1291.8390	1283.3342	1269.2371	1247.9675	1215.7333
	3	2434.5770	2452.9625	2448.6216	2432.2843	2411.2829	2397.2279	2391.1039	2393.1465	2393.0364	2383.8683	2355.2590

Table 14. Comparison between the first three natural frequencies of anti-symmetric and symmetric VSCL and CSCL beam with the boundary conditions: S-S.

Lay-up	Mode	T_1										
VSCL		$\langle 0,-25\rangle$	$\langle 0,-20\rangle$	$\langle 0,-15\rangle$	$\langle 0,-10\rangle$	$\langle 0,-5\rangle$	0	$\langle 0,5\rangle$	$\langle 0,10\rangle$	$\langle 0,15\rangle$	$\langle 0,20\rangle$	$\langle 0,25\rangle$
$[45_3,\pm\langle T_0,T_1\rangle_2]$	1	398.0499	399.1262	399.5111	399.4924	399.3425	399.2666	399.3425	399.4924	399.5111	399.1262	398.0449
	2	1313.2691	1317.4637	1317.9173	1316.3416	1314.4697	1313.6691	1314.4697	1316.3416	1317.9173	1317.4637	1313.2691
	3	2432.2927	2424.9692	2413.8728	2402.2043	2393.3464	2390.0363	2393.3464	2402.2043	2413.8728	2424.9692	2432.2927
CSCL		$\langle -25,-25\rangle$	$\langle -20,-20\rangle$	$\langle -15,-15\rangle$	$\langle -10,-10\rangle$	$\langle -5,-5\rangle$	0	$\langle 5,5\rangle$	$\langle 10,10\rangle$	$\langle 15,15\rangle$	$\langle 20,20\rangle$	$\langle 25,25\rangle$
$[45_3,\pm\langle T_0,T_1\rangle_2]$	1	361.8693	376.4226	386.9631	394.1572	397.8544	399.2666	397.9933	394.4177	387.3151	376.8353	362.3162
	2	1269.2182	1297.2280	1310.8497	1315.2917	1313.9985	1313.6691	1314.3986	1316.0569	1311.9134	1298.5164	1270.6602
	3	2437.0380	2451.2371	2440.7622	2419.2289	2397.5532	2390.0363	2398.1939	2420.5254	2442.5086	2453.3985	2439.5214
VSCL		$\langle 0,-25\rangle$	$\langle 0,-20\rangle$	$\langle 0,-15\rangle$	$\langle 0,-10\rangle$	$\langle 0,-5\rangle$	0	$\langle 0,5\rangle$	$\langle 0,10\rangle$	$\langle 0,15\rangle$	$\langle 0,20\rangle$	$\langle 0,25\rangle$
$[45_3,\pm\langle T_0,T_1\rangle_s]$	1	398.0457	399.1267	399.5115	399.4925	399.3425	399.2666	399.2425	399.5115	399.5115	399.1267	399.0457
	2	1313.2730	1317.4665	1317.9190	1316.3425	1314.4699	1313.6691	1314.4699	1316.3425	1317.9190	1317.4665	1313.2730
	3	2432.2989	2424.9738	2413.8757	2402.2057	2393.3467	2393.3467	2393.3467	2402.2057	2413.8757	2424.9738	2432.2989
CSCL		$\langle -25,-25\rangle$	$\langle -20,-20\rangle$	$\langle -15,-15\rangle$	$\langle -10,-10\rangle$	$\langle -5,-5\rangle$	0	$\langle 5,5\rangle$	$\langle 10,10\rangle$	$\langle 15,15\rangle$	$\langle 20,20\rangle$	$\langle 25,25\rangle$
$[45_3,\pm\langle T_0,T_1\rangle_s]$	1	362.0975	376.6332	387.1424	394.2896	397.9248	399.2666	397.9232	394.2866	387.1384	376.6285	362.0925
	2	1269.9546	1297.8853	1311.3916	1315.6807	1314.2013	1313.6691	1314.1968	1315.6721	1311.3796	1297.8708	1269.9384
	3	2438.3064	2452.3399	2441.6518	2419.9174	2397.8781	2390.0363	2397.8709	2419.9035	2441.6322	2452.3156	2438.2785

Table 15. Comparison between the first three natural frequencies of anti-symmetric and symmetric VSCL and CSCL beam with the boundary conditions: S-S.

Lay-up	Mode	T_1										
VSCL		$\langle 0, -25\rangle$	$\langle 0, -20\rangle$	$\langle 0, -15\rangle$	$\langle 0, -10\rangle$	$\langle 0, -5\rangle$	0	$\langle 0, 5\rangle$	$\langle 0, 10\rangle$	$\langle 0, 15\rangle$	$\langle 0, 20\rangle$	$\langle 0, 25\rangle$
$[45_3/\pm\langle T_0, T_1\rangle_3]$	1	412.7516	413.3999	413.2409	412.6762	412.1139	411.8832	412.1139	412.6762	413.2409	413.3999	412.7516
	2	1332.3662	1333.8283	1331.1226	1326.4553	1322.2583	1320.5843	1322.2583	1326.4553	1331.1226	1333.8283	1332.3662
	3	2430.3019	2414.9697	2395.9052	2377.1176	2363.1723	2357.9939	2363.1723	2377.1176	2395.9052	2414.9697	2430.3019
CSCL		$\langle -25, -25\rangle$	$\langle -20, -20\rangle$	$\langle -15, -15\rangle$	$\langle -10, -10\rangle$	$\langle -5, -5\rangle$	0	$\langle 5, 5\rangle$	$\langle 10, 10\rangle$	$\langle 15, 15\rangle$	$\langle 20, 20\rangle$	$\langle 25, 25\rangle$
$[45_3/\pm\langle T_0, T_1\rangle_3]$	1	373.9206	389.5253	400.3954	407.3987	410.6697	411.8832	410.7709	407.7709	400.6453	389.8141	374.2297
	2	1299.2307	1324.7179	1332.8209	1330.4043	1323.2188	1320.5843	1323.4963	1330.9322	1333.5500	1325.5957	1300.2092
	3	2472.8294	2474.4519	2446.5910	2406.8768	2370.8723	2357.9939	2371.3098	2407.7154	2447.7666	2475.8990	2474.4891
VSCL		$\langle 0, -25\rangle$	$\langle 0, -20\rangle$	$\langle 0, -15\rangle$	$\langle 0, -10\rangle$	$\langle 0, -5\rangle$	$\langle 0, 0\rangle$	$\langle 0, 5\rangle$	$\langle 0, 10\rangle$	$\langle 0, 15\rangle$	$\langle 0, 20\rangle$	$\langle 0, 25\rangle$
$[45_3, (+\langle T_0, T_1\rangle,$	1	411.8400	412.7568	412.8443	412.4856	412.0636	411.8832	412.0636	412.4856	412.8443	412.7568	411.8400
$-\langle T_0, T_1\rangle,$	2	1327.9977	1330.6235	1329.1157	1325.4720	1321.9956	1320.5843	1321.9956	1325.4720	1329.1157	1330.6535	1327.9977
$+\langle T_0, T_1\rangle)_s]$	3	2423.6485	2410.0333	2329.7237	2375.5335	2362.7446	2357.9939	2362.7446	2375.5335	2392.7237	2410.0333	2423.6485
CSCL		$\langle -25, -25\rangle$	$\langle -20, -20\rangle$	$\langle -15, -15\rangle$	$\langle -10, -10\rangle$	$\langle -5, -5\rangle$	$\langle 0, 0\rangle$	$\langle 5, 5\rangle$	$\langle 10, 10\rangle$	$\langle 15, 15\rangle$	$\langle 20, 20\rangle$	$\langle 25, 25\rangle$
$[45_3, (+\langle T_0, T_1\rangle,$	1	377.3786	392.9979	403.7360	410.2384	412.4145	411.8832	408.5658	403.0930	394.2042	381.9641	365.5533
$-\langle T_0, T_1\rangle,$	2	1310.1614	1335.2537	1342.5481	1338.3773	1327.9979	1320.5843	1317.4379	1318.2498	1314.6773	1301.6305	1272.6277
$+\langle T_0, T_1\rangle)_s]$	3	2491.3509	2491.8090	2462.2700	2419.5432	2378.4069	2357.9939	2361.7619	2387.5678	2417.3111	2436.3139	2427.5748

Table 16. Comparison between the first three natural frequencies of anti-symmetric and symmetric VSCL and CSCL beam with the boundary conditions: S-S.

Lay-up		T_1										
VSCL	Mode	$\langle 0,-25\rangle$	$\langle 0,-20\rangle$	$\langle 0,-15\rangle$	$\langle 0,-10\rangle$	$\langle 0,-5\rangle$	0	$\langle 0,5\rangle$	$\langle 0,10\rangle$	$\langle 0,15\rangle$	$\langle 0,20\rangle$	$\langle 0,25\rangle$
$[45_3/\pm\langle T_0,T_1\rangle_4]$	1	421.0030	421.2550	420.6134	419.5645	418.6327	418.2622	418.6327	419.5645	420.6134	421.2550	421.0030
	2	1338.8868	1338.2080	1333.0558	1325.9680	1319.9183	1317.5397	1319.9183	1325.9680	1333.0558	1338.2080	1338.8868
	3	2418.9508	2397.8693	2373.0802	2349.1099	2331.3957	2324.8166	2331.3957	2349.1099	2373.0802	2397.8693	2418.9508
CSCL		$\langle -25,-25\rangle$	$\langle -20,-20\rangle$	$\langle -15,-15\rangle$	$\langle -10,-10\rangle$	$\langle -5,-5\rangle$	0	$\langle 5,5\rangle$	$\langle 10,10\rangle$	$\langle 15,15\rangle$	$\langle 20,20\rangle$	$\langle 25,25\rangle$
$[45_3,\pm\langle T_0,T_1\rangle_4]$	1	380.8693	396.9782	407.8487	414.4847	417.2664	418.2622	417.3423	414.6243	408.0327	397.1886	381.0926
	2	1315.4885	1338.5177	1342.0191	1334.0175	1322.0500	1317.5397	1322.2515	1334.3991	1342.5437	1339.1464	1316.1873
	3	2490.2257	2482.3445	2441.6108	2388.3693	2341.7112	2324.8166	2342.0269	2388.9709	2442.4487	2483.3710	2491.4006
VSCL		$\langle 0,-25\rangle$	$\langle 0,-20\rangle$	$\langle 0,-15\rangle$	$\langle 0,-10\rangle$	$\langle 0,-5\rangle$	0	$\langle 0,5\rangle$	$\langle 0,10\rangle$	$\langle 0,15\rangle$	$\langle 0,20\rangle$	$\langle 0,25\rangle$
$[45_3,\pm\langle T_0,T_1\rangle_{2s}]$	1	421.0035	421.2554	420.6137	419.5646	418.6328	418.2622	418.6328	419.5646	420.6137	421.2554	421.0035
	2	1338.8891	1338.2097	1333.0569	1325.9685	1319.9184	1317.5397	1319.9184	1325.9685	1333.0569	1338.2097	1338.8891
	3	2418.9543	2397.8719	2373.0819	2349.1107	2331.3959	2324.8166	2331.3959	2349.1107	2373.0819	2397.8719	2418.9543
CSCL		$\langle -25,-25\rangle$	$\langle -20,-20\rangle$	$\langle -15,-15\rangle$	$\langle -10,-10\rangle$	$\langle -5,-5\rangle$	0	$\langle 5,5\rangle$	$\langle 10,10\rangle$	$\langle 15,15\rangle$	$\langle 20,20\rangle$	$\langle 25,25\rangle$
$[45_3,\pm\langle T_0,T_1\rangle_{2s}]$	1	380.9840	397.0861	407.9429	414.5560	417.3050	418.2622	417.3039	414.5540	407.9402	397.0831	380.9807
	2	1315.8474	1338.8402	1342.2877	1334.2123	1322.1526	1317.5397	1322.1497	1334.2069	1342.2801	1338.8311	1315.8374
	3	2438.3064	2482.8711	2442.0397	2388.6764	2341.8719	2324.8166	2341.8673	2388.6678	2442.0277	2482.8563	2490.8122

Table 17. The first three natural frequencies of a symmetric VSCL beam $[+\langle T_0, T_1\rangle, -\langle T_0, T_1\rangle]$, with the different boundary conditions and $T_0 = 0$.

		T_1										
Boundary conditions	mode	−25	−20	−15	−10	−5	0	5	10	15	20	25
C-C	1	723.1765	706.1111	685.1353	664.0599	647.9347	641.8078	647.9347	664.0599	685.1353	706.1111	723.1765
	2	1543.1155	1490.7686	1432.2633	1376.6346	1335.5116	1320.1580	1335.5116	1376.6346	1432.2633	1490.7686	1543.1155
	3	2443.8164	2352.7252	2260.1915	2177.2123	2117.9890	2096.2473	2117.9890	2177.2123	2260.1915	2352.7252	2443.8164
C-F	1	158.5036	162.2288	164.6968	166.1237	166.7558	166.9639	168.7858	166.1237	164.6968	162.2288	158.5036
	2	804.2260	787.0921	767.2922	747.9407	733.3034	727.7625	733.3034	747.9407	767.2922	787.0921	804.2260
	3	1714.5765	1677.4496	1634.6918	1593.1917	1562.1219	1550.4549	1562.1219	1593.1917	1634.6918	1677.4496	1714.5765

Table 18. The first three natural frequencies of a symmetric VSCL beam $[+\langle T_0, T_1\rangle, -\langle T_0, T_1\rangle + \langle T_0, T_1\rangle]$ with the different boundary conditions and $T_0 = 0$.

		T_1										
Boundary conditions	mode	−25	−20	−15	−10	−5	0	5	10	15	20	25
C-C	1	719.7145	703.4275	683.3106	663.0963	647.6612	641.8078	647.6612	663.0963	683.3106	703.4275	719.7145
	2	1537.4233	1486.4902	1429.4095	1375.1406	1335.0883	1320.1580	1335.0883	1375.1406	1429.4095	1486.4902	1537.4233
	3	2433.5908	2344.8885	2254.9099	2174.4452	2117.2085	2096.2473	2117.2085	2174.4452	2254.9099	2344.8885	2433.5908
C-F	1	157.1317	161.1496	163.9615	165.7384	166.6777	166.9639	166.6777	165.7384	163.9615	161.1496	157.1317
	2	801.1753	784.8453	765.8302	747.1940	733.0957	727.7625	733.0957	747.1940	765.8302	784.8453	801.1753
	3	1707.1358	1671.9152	1631.0589	1591.3274	1561.6031	1550.4549	1561.6031	1591.3274	1631.0589	1671.9152	1707.1358

Table 19. The first three natural frequencies of a symmetric VSCL beam $[+\langle T_0, T_1\rangle, -\langle T_0, T_1\rangle, +\langle T_0, T_1\rangle, -\langle T_0, T_1\rangle]$ with the different boundary conditions and $T_0 = 0$.

		T_1										
Boundary conditions	mode	−25	−20	−15	−10	−5	0	5	10	15	20	25
C-C	1	723.2140	706.1402	685.1552	664.0704	647.9377	641.8078	647.9377	664.0704	685.1552	706.1402	723.2140
	2	1543.1771	1490.8150	1432.2943	1376.6509	1335.5162	1320.1580	1335.5162	1376.6509	1432.2943	1490.8150	1543.1771
	3	2443.9274	2352.8103	2260.2489	2177.2425	2117.9975	2096.2473	2117.9975	2177.2425	2260.2489	2352.8103	2443.9274
C-F	1	158.5185	162.2405	164.7048	166.1279	166.7870	166.9639	166.7870	166.1279	164.7048	162.2405	158.5185
	2	804.2590	787.1164	767.3080	747.9488	733.3056	727.7625	733.3056	747.9488	767.3080	787.1164	804.2590
	3	1714.6571	1677.5096	1634.7313	1593.2121	1562.1276	1550.4549	1562.1276	1593.2121	1634.7313	1677.5096	1714.6571

Table 20. The first three natural frequencies of a symmetric VSCL beam $[+\langle T_0, T_1\rangle, -\langle T_0, T_1\rangle, -\langle T_0, T_1\rangle, +\langle T_0, T_1\rangle]$ with the different boundary conditions and $T_0 = 0$.

		T_1										
Boundary conditions	mode	−25	−20	−15	−10	−5	0	5	10	15	20	25
C-C	1	723.2265	706.1499	685.1618	664.0739	647.9387	641.8078	647.9387	664.0739	685.1618	706.1499	723.2265
	2	1543.1976	1490.8304	1432.3046	1376.6563	1335.5177	1320.1580	1335.5177	1376.6563	1432.3046	1490.8304	1543.1976
	3	2443.9643	2352.8386	2260.2680	2177.2525	2118.0003	2096.2473	2118.0003	2177.2525	2260.2680	2352.8386	2443.9643
C-F	1	158.5235	162.2444	164.7075	166.1293	166.7874	166.9639	166.7874	166.1293	164.7075	162.2444	158.5235
	2	804.2701	787.1246	767.3133	747.9515	733.3064	727.7625	733.3064	747.9515	767.3133	787.1246	804.2701
	3	1714.6839	1677.5296	1634.7445	1593.2188	1562.1295	1550.4549	1562.1295	1593.2188	1634.7445	1677.5296	1714.6839

properties of materials used in the last previous example are utilized. The same fiber orientation angle of VSCL like the previous example are used, in which the fiber orientation angle T_0 keep to zero; whereas the fiber orientation T_1 varies from -25 to 25. In the case of the CSCL, the fiber orientation angle is constant, it mean that the fiber orientation angle T_0 and T_1 is identical ($T_0 = T_1$).

Tables 13–16 show that, the first frequency is increased when the fiber orientation angle T_1 increases from -25 to 25 by 9.434% for two layers, 7.145% for three layers, 9.089% for four anti-symmetric layers, 9.031% for four symmetric layers, 9.408% for six anti-symmetric layers, 8.368% for six symmetric layers, 9.533% for eight anti-symmetric layers, 9.506% for eight symmetric layers respectively. It clearly show that the natural frequency of the constant stiffness composite beam is very less than the natural frequency of variable stiffness composite beam, that is to say the VSCL beam is most stiffness than the CSCL beam.

Tables 17–20 gives the effect of boundary conditions on the first three natural frequencies of a VSCL beam with $[\pm\langle T_0, T_1\rangle]$ lay-ups varies to two, three and four symmetric and anti-symmetric layers respectively. In addition of the first boundary condition used in the first example (see Table 10), we used others boundary conditions like to C-C and C-F respectively, in which the symbol C-C denote the clamped-clamped boundary condition and C-F denote the clamped-free boundary condition.

In the case of the effect of the boundary condition C-C, the first natural frequency of the fourth laminates is increased by 11.252%, 10.825%, 11.311% and 11.258% respectively. In the second case of the effect of the boundary condition C-F the first natural frequency of the fourth laminates is decreased by 5.338%, 6.257, 5.328% and 5.324% whereas, in the case of simply-supported (see in the Table 10) the first natural is increased by 4.373%, 3.9%, 4.378% and 4.379% respectively for the four variable stiffness

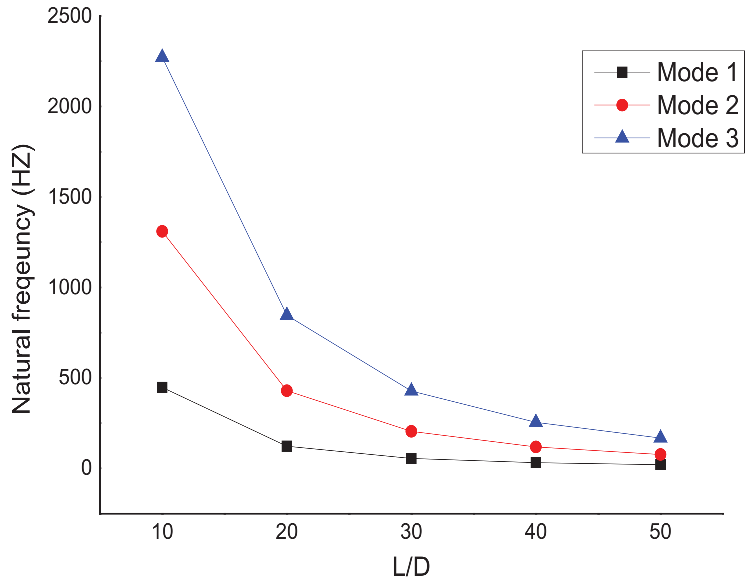

Figure 18. The first three natural frequencies of $[\pm\langle 0, 25\rangle]$ laminate, for simply supported S-S beam, L/D variable.

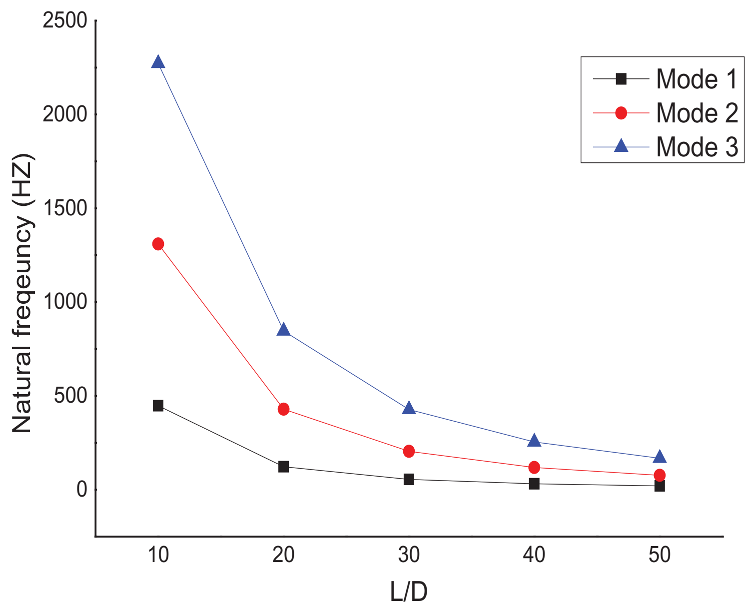

Figure 19. The first three natural frequencies of $[+\langle 0, 25\rangle, -\langle 0, 25\rangle, +-\langle 0, 25\rangle]$ laminate, for simply supported S-S beam, L/D variable.

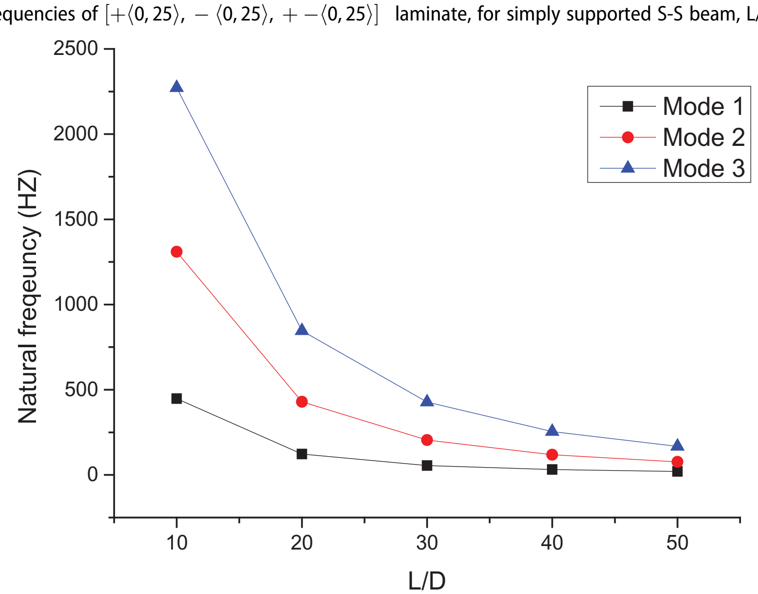

Figure 20. The first three natural frequencies of $\pm\langle 0, 25\rangle_2$ laminate, for simply supported S-S beam, L/D variable.

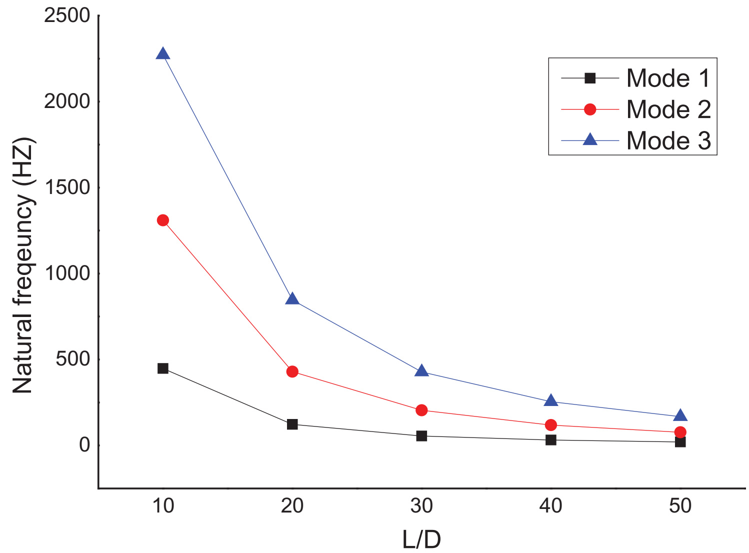

Figure 21. The first three natural frequencies of $\pm\langle 0, 25\rangle_s$ laminate, for simply supported S-S beam, L/D variable.

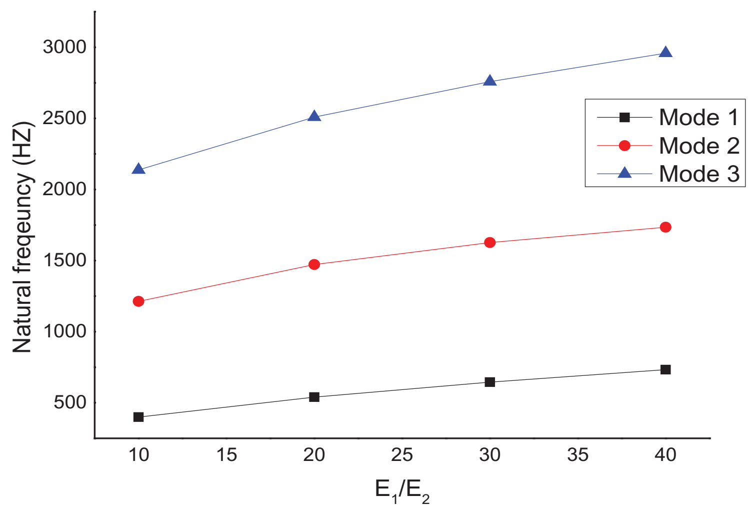

Figure 22. The first three natural frequencies of $[\pm\langle 0, 25\rangle]$ laminate, for simply supported S-S Beam, E_1/E_2 variable.

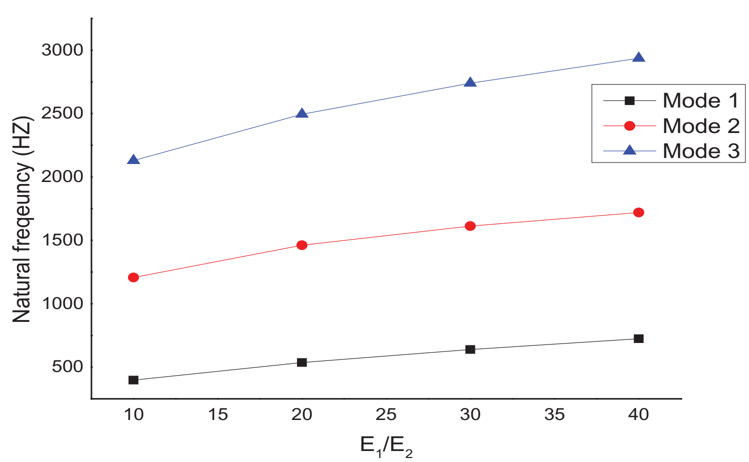

Figure 23. The first three natural frequencies of $[+\langle 0, 25\rangle, -\langle 0, 25\rangle, +\langle 0, 25\rangle]$ laminate, for simply supported S-S beam, E_1/E_2 variable.

composite beams. It can be concluded that the variable stiffness composite beams are more stiffener in the cases of S-S and C-C boundary conditions than in the case of C-F boundary conditions.

Figures 18–21 gives the first natural frequency for VSCL beam with $[\pm\langle T0, T1\rangle]$ lay-ups varying with the length to mean diameter ratios (L/D), in which the length to mean diameter ratio varies from 10 to 50, and the fiber orientation

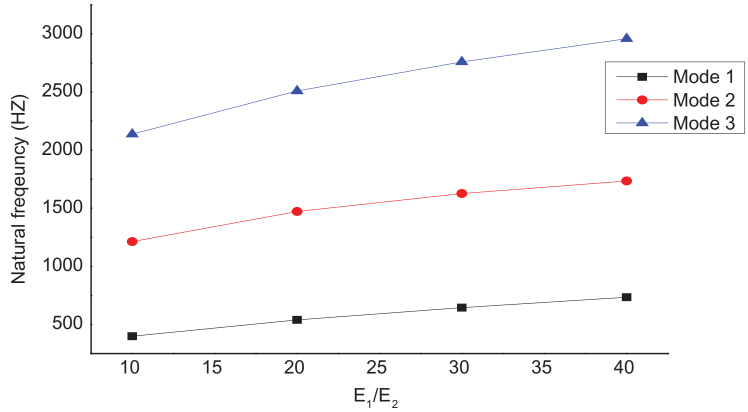

Figure 24. The first three natural frequencies of $\pm\langle 0, 25\rangle_2$ laminate, for simply supported S-S Beam, E_1/E_2 variable.

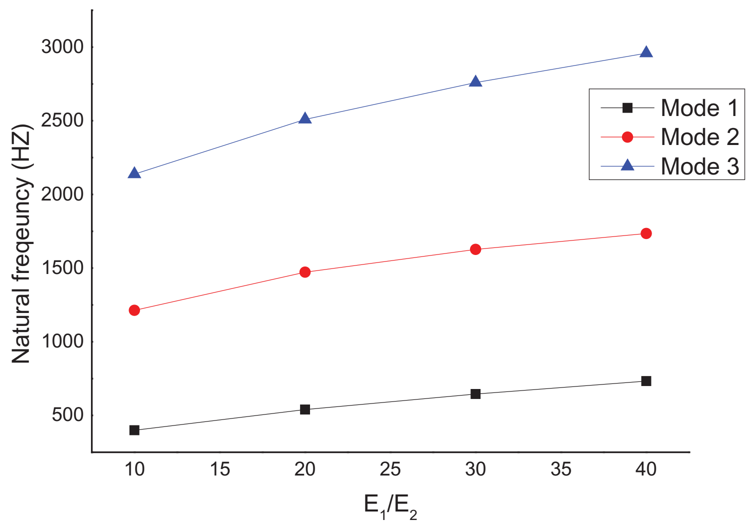

Figure 25. The first three natural frequencies of $\pm\langle 0, 25\rangle_s$ laminate, for simply supported S-S beam, E_1/E_2 variable.

parabolic angle T_0 and T_1 keep to 0 and 25 respectively for examples of laminates; two, three, and four symmetric and anti-symmetric layers, it can be observed that the natural frequency is decreased when the length to mean diameter ratios are increased.

Figures 22–25 gives the first natural frequency for VSCL beam with $[\pm\langle T0, T1\rangle]$ lay-ups varying with the modulus elasticity (E_1/E_2), in which the modulus ratio varies from 10 to 40, and the fiber orientation parabolic angle T_0 and T_1 keep to 0° and 25° respectively for four laminates; two, three, and four symmetric and anti-symmetric layers, it can be observed that the natural frequency is increased when the modulus elasticity ratios are increased.

7. Conclusion

The free vibration analysis of variable stiffness composite beams with parabolic fibers have been presented using the Equivalent Single Layer Theory (ESLT) in conjunction with the iso-geometric approach. The present theory includes both stretching, shearing, bending and twisting effects. A new iso-geometric composite beam element with six degrees of freedom per control point has been developed. This study allowed us to reach the following conclusions:

1. For different results, the convergence of the solution is ensured by increasing the number of elements or the degrees of basic functions. Highly accurate values are obtained with the use of a very few degrees of freedoms, in which h-, p- and k-refinement are used in the convergence analysis. It is found that the proposed approach can yield highly accurate solutions compared to other existing methods available in the literature.
2. The vibration behavior of VSCL beams are influenced significantly by the parabolic fiber orientation (symmetric, anti-symmetric), the stacking sequence and the length to mean diameter ratio, the modulus ratio, and different the boundary conditions.
3. The natural frequencies increase with the increment of the fiber orientation angle, the number of layers, and the stacking sequence, in which the fiber orientation angle T_0 keep to zero and decreasing when the fiber orientation angle T_0 is difference to zero.
4. A comparison study is investigated between the VSCL beams and the CSCL beams. It clearly shown that the VSCL beams has higher stiffener than the CSCL beams.
5. The natural frequencies is influenced by the variation of boundary conditions, in which the natural frequency become large for S-S and C-C boundary conditions, and

the contrast is produced in the case of C-F boundary condition.
6. The natural frequencies is also influenced by the variation of the length to mean diameter ratio, the modulus ratios, in which the natural frequency is increased with the increment of the modulus ratio and decreased with the increment of length-diameter ratio.

References

[1] K. K. Teh and C. C. Huang, The vibrations of generally orthotropic beams, a finite element approach, J. Sound Vib., vol. 62, no. 2, pp. 195–206, 1979. DOI: 10.1016/0022-460X(79)90021-X.
[2] K. Chandrashekhara, K. Krishnamurthy, and S. Roy, Free vibration of composite beams including rotary inertia and shear deformation, Compos. Struct., vol. 14, no. 4, pp. 269–279, 1990. DOI: 10.1016/0263-8223(90)90010-C.
[3] M. Eisenberger, H. Abramovich, and O. Shulepov, Dynamic stiffness analysis of laminated beams using a first order shear deformation theory, Compos. Struct., vol. 31, no. 4, pp. 265–271, 1995. DOI: 10.1016/0263-8223(95)00091-7.
[4] J. R. Bannerjee, and F. W. Williams, Exact dynamic stiffness matrix for composite Timoshenko beams with applications, J. Sound Vib., vol. 194, no. 4, pp. 573–585, 1996. DOI: 10.1006/jsvi.1996.0378.
[5] S. P. Singh, and K. Gupta, Composite shaft rotor dynamic analysis using a layer wise theory, J. Sound Vib., vol. 191, no. 5, pp. 739–756, 1996. DOI: 10.1006/jsvi.1996.0153.
[6] H. Gubran and K. Gupta, The effect of stacking sequence and coupling mechanisms on the natural frequencies of composite shafts, J. Sound Vib., vol. 282, no. 1-2, pp. 231–248, 2005. DOI: 10.1016/j.jsv.2004.02.022.
[7] M. Tahani, Analysis of laminated composite beams using layerwise displacement theories, Compos. Struct., vol. 79, no. 4, pp. 535–547, 2007. vol DOI: 10.1016/j.compstruct.2006.02.019.
[8] M.-Y. Chang, J.-K. Chen, and C.-Y. Chang, A simple spinning laminated composite shaft model, Int. J. Solids Struct., vol. 41, no. 3-4, pp. 637–662, 2004. DOI: 10.1016/j.ijsolstr.2003.09.043.
[9] A. Boukhalfa, A. Hadjoui, and S. M. Hamza-Cherif, Free vibration analysis of a rotating composite shaft using the p-version of the finite element method, Int. J. Rotat. Mach., vol. 2008, pp. 1–10, 2008. DOI: 10.1155/2008/752062.
[10] E. Carrera, M. Filippi, and E. Zappino, Laminated beam analysis by polynomial, trigonometric, exponential and zig-zag theories, Eur. J. Mech. A, vol. 41, pp. 58–69, 2013. DOI: 10.1016/j.euromechsol.2013.02.006.
[11] S. Ben Arab, J. D. Rodrigues, S. Bouaziz, and M. Haddar, A finite element based on equivalent single layer theory for rotating composite shafts dynamic analysis, Compos. Struct., vol. 178, pp. 135–144, 2017. DOI: 10.1016/j.compstruct.2017.06.052.
[12] R. B. Abarcar and P. F. Cunniff, The vibration of cantilever beams of fiber reinforced material, J. Compos. Mater., vol. 6, no. 4, pp. 504–517, 1972. DOI: 10.1177/002199837200600306.
[13] L. S. Teoh and C. C. Huang, The vibration of beams of fiber reinforced material, J. Vib. Acoust., vol. 51, pp. 467–473, 1977. DOI: 10.1016/S0022-460X(77)80044-8.
[14] L. S. Teoh and C. C. Huang, The effects of fiber orientation on free vibration of composite beams, J. Vib. Acoust., vol. 69, pp. 327–337, 1980. DOI: 10.1016/0022-460X(80)90616-1.
[15] V. Yildirim, Effects of the longitudinal to transverse moduli ratio on the in-plane natural frequencies of symmetric cross ply laminated beams by the stiffness method, J. Compos. Mater., vol. 50, pp. 319–326, 2000.
[16] G. Rajeshkumar and V. Hariharan, Free vibration analysis of hybrid-composite beams, IEEE-International Conference on Advances in Engineering, Science and Management, ICESM, Nagapattinam, Tamil Nadu, India, 2012.
[17] J. H. Khatri, H. P. Patolia, and K. B. Brahmbhatt, Analysis of mechanical properties of natural fiber composite beam, Kapla Publ. Eng., vol. 1, pp. 233–238, 2017.
[18] A. W. Leissa and A. F. Martin, Vibration and buckling of rectangular composite plates with variable fiber spacing, Compos. Struct., vol. 14, no. 4, pp. 339–357, 1990. DOI: 10.1016/0263-8223(90)90014-6.
[19] M. W. Hyer and H. H. Lee, The use of curvilinear fiber format to improve buckling resistance of composite plates with central circular holes, Compos. Struct., vol. 18, no. 3, pp. 239–261, 1991. DOI: 10.1016/0263-8223(91)90035-W.
[20] S. Honda, Y. Oonishi, Y. Narita, and K. Sasaki, Vibration analysis of composite rectangular plates reinforced along curved lines, J. Syst. Des. Dyn., vol. 2, no. 1, pp. 76–86, 2008. DOI: 10.1299/jsdd.2.76.
[21] S. Honda and Y. Narita, Natural frequencies and vibration modes of laminated composite plates reinforced with arbitrary curvilinear fiber shape paths, J. Sound Vib., vol. 331, no. 1, pp. 180–191, 2012. DOI: 10.1016/j.jsv.2011.08.019.
[22] H. Akhavan and P. Ribeiro, Natural modes of vibration of variable stiffness composite laminates with curvilinear fibers, Compos. Struct., vol. 93, no. 11, pp. 3040–3047, 2011. DOI: 10.1016/j.compstruct.2011.04.027.
[23] P. Ribeiro and H. Akhavan, Non-linear vibrations of variable stiffness composite laminated plates, Compos. Struct., vol. 94, no. 8, pp. 2424–2432, 2012. DOI: 10.1016/j.compstruct.2012.03.025.
[24] H. Akhavan, P. Ribeiro, and M. F. S. F. de Moura, large deflection and stress in variable stiffness composite laminates with curvilinear fibers, Int. J. Mech. Sci., vol. 73, pp. 14–26, 2013. DOI: 10.1016/j.ijmecsci.2013.03.013.
[25] S. Yazdani, P. Ribeiro, and J. D. Rodrigues, A p-version layerwise model for large deflection of composite laminates with curvilinear fibers, Compos. Struct., vol. 108, pp. 181–190, 2014. DOI: 10.1016/j.compstruct.2013.09.014.
[26] S. Yazdani and P. Ribeiro, A layer-wise p-version finite element formulation for free vibration analysis of thick composite laminates with curvilinear fibers, Compos. Struct., vol. 120, pp. 531–542, 2015. DOI: 10.1016/j.compstruct.2014.10.030.
[27] A. Houmat, Non-linear free vibrations of laminated composite rectangular plates with curvilinear fibers, Compos. Struct., vol. 106, pp. 211–224, 2013. DOI: 10.1016/j.compstruct.2013.05.058.
[28] M. Hachemi, S. M. Hamza-Cherif, and A. Houmat, Free vibration analysis of variable stiffness composite laminate plate with circular cutout, Aust. J. Mech. Eng., pp. 1–17, 2017. DOI: 10.1080/14484846.2017.1385694.
[29] S. M. N. Serdoun and S. M. Hamza-Cherif, Vibration analysis of composite and sandwich plates reinforced with parabolic fibers using an alternative hierarchical finite element method, J. Sandwich. Struct. Mater, pp. 0542–1878, 2018. DOI: 10.1177/1099636218780542
[30] M. Hachemi, Vibration analysis of variable stiffness laminated composite sandwich plates, Mech. Adv. Mater. Struct., pp. 1–15, 2019. DOI: 10.1080/15376494.2018.1524951.
[31] A. Bendahmane, S. M. Hamza-Cherif, and M. N. Ouissi, Free vibration analysis of variable stiffness composite laminate (VSCL) plates coupled with fluid, Mech. Adv. Mater. Struct, pp. 1–16, 2019. DOI: 10.1080/15376494.2018.1553257.
[32] Z. Zamani, H. Haddadpour, and M. R. Ghazavi, Curvilinear fiber optimization tools for design thin walled beams, Thin-Wall. Struct., vol. 49, no. 3, pp. 448–454, 2011. DOI: 10.1016/j.tws.2010.08.002.
[33] H. Haddadpour and Z. Zamani, Curvilinear fiber optimization tools for aeroelastic design of composite wings, J. Fluids Struct., vol. 33, pp. 180–190, 2012. DOI: 10.1016/j.jfluidstructs.2012.05.008.
[34] A. Boukhalfa, Campbell diagrams of a spinning composite shaft with curvilinear fibers, Latin Am. J. Solids Struct., vol. 14, no. 4, pp. 575–593, 2017. DOI: 10.1590/1679-78253326.
[35] T. J. R. Hughes, J. A. Cottrell, and Y. Bazilevs, Isogeometric analysis: CAD, finite elements, NURBS, exact geometry and mesh refinement, Comput. Methods Appl. Mech. Eng., vol. 194, no. 39-41, pp. 4135–4195, 2005.

[36] J. A. Cottrell, Y. Bazilevs, and T. J. R. Hughes, Isogeometric Analysis: Towards Integration of CAD and FEA, Wiley, John Wiley & Sons, Chichester, United Kingdom, 2009.
[37] X. Xu, B. Kargoll, J. Bureick, H. Yang, H. Alkhatib, and I. Neumann, TLS-based profile model analysis of major composite structures with robust B-spline method, Compos. Struct., vol. 184, pp. 814–820, 2018. DOI: 10.1016/j.compstruct.2017.10.057.
[38] H. Yang and X. Xiangyang, Multi-sensor technology for B-spline modeling and deformation analysis of composite structures, Compos. Struct., vol. 224, pp. 111000, 2019. DOI: 10.1016/j.compstruct.2019.111000.
[39] H. Yang, X. Xu, B. Kargoll, and I. Neumann, An automatic and intelligent optimal surface modelling method for composite tunnel structures, Compos. Struct., vol. 208, pp. 702–710, 2019. DOI: 10.1016/j.compstruct.2018.09.082.
[40] X. Xu, H. Yang, R. Augello, and E. Carrera, Optimized free-form surface of point clouds from laser-based measurement, Mech. Adv. Mater. Struct, pp. 1–10, 2019. DOI: 10.1080/15376494.2019.1688435.
[41] X. Xu, R. Augello, and H. Yang, The generation and validation of a CUF-based FEA model with laser-based experiments, Mech. Adv. Mater. Struct, pp. 1–9, 2019. DOI: 10.1080/15376494.2019.1697473.
[42] J. A. Cottrell, A. Reali, Y. Bazilevs, and T. J. R. Hughes, Isogeometric analysis of structural vibrations, Comput. Methods Appl. Mech. Eng., vol. 195, no. 41-43, pp. 5257–5296, 2006. DOI: 10.1016/j.cma.2005.09.027.
[43] S. J. Lee and K. S. Park, Vibrations of Timoshenko beams with isogeometric approach, Appl. Math. Model., vol. 37, no. 22, pp. 9174–9190, 2013. DOI: 10.1016/j.apm.2013.04.034.
[44] S. Faroughi, E. Shafei, and A. Eriksson, NURBS-based modeling of laminated composite beams with isogeometric displacement-only theory, Compos. Struct. Part B, vol. 162, pp. 89–102, 2019. DOI: 10.1016/j.compositesb.2018.10.073.
[45] X. Wang, X. Zhu, and P. Hu, Isogeometric finite element method for buckling analysis of generally laminated composite beams with different boundary conditions, Int. J. Mech. Sci., vol. 104, pp. 190–199, 2015. DOI: 10.1016/j.ijmecsci.2015.10.008.
[46] D. J. Benson, Y. Bazilevs, M. C. Hsu, and T. J. R. Hughes, Isogeometric shell analysis: The Reissner–Mindlin shell, Comput. Methods Appl. Mech. Eng., vol. 199, no. 5-8, pp. 276–289, 2010. DOI: 10.1016/j.cma.2009.05.011.
[47] J. Kiendl, K. U. Bletzinger, J. Linhard, and R. Wuchner, Isogeometric shell analysis with Kirchhoff–Love elements, Comput. Methods Appl. Mech. Eng., vol. 198, no. 49-52, pp. 3902–3914, 2009. DOI: 10.1016/j.cma.2009.08.013.
[48] S. Shojaee, E. Izadpanah, N. Valizadeh, and J. Kiendl, Free vibration analysis of thin plates by using a NURBS-based isogeometric approach, Int. J. Finite Elem. Anal. Des., vol. 61, pp. 23–34, 2012. DOI: 10.1016/j.finel.2012.06.005.
[49] Q. X. Lieu, D. Lee, J. Kang, and J. Lee, NURBS-based modeling and analysis for free vibration and buckling problems of in-plane bidirectional functionally graded plates, Mech. Adv. Mater. Struct, pp. 1–17, 2018. DOI:10.1080/15376494.2018.1430273.
[50] N. Liu and A. E. Jeffers, Isogeometric analysis of laminated composite and functionally graded sandwich plates based on a layer wise displacement theory, Compos. Struct., vol. 176, pp. 143–153, 2017. DOI: 10.1016/j.compstruct.2017.05.037.
[51] N. Liu and A. E. Jeffers, Adaptive isogeometric analysis in structural frames using a layer-based discretization to model spread of plasticity, Comput. Struct., vol. 196, pp. 1–11, 2018.vol DOI: 10.1016/j.compstruc.2017.10.016.
[52] N. Liu and A. E. Jeffers, A geometrically exact isogeometric Kirchhoff plate: feature-preserving automatic meshing and C1 rational triangular Bezier spline discretizations, Int. J. Numer. Methods Eng., vol. 115, no. 3, pp. 395–409, 2018. DOI: 10.1002/nme.5809.
[53] W. A. Wall, M. A. Frenzel, and C. Cyron, Full analytical sensitivities in NURBS based isogeometric shape optimization, Comput. Methods Appl. Mech. Eng., vol. 197, no. 33-40, pp. 2976–2988, 2008. DOI: 10.1016/j.cma.2008.01.025.
[54] X. Qian, Isogeometric structural shape optimization, Comput. Methods Appl. Mech. Eng., vol. 199, no. 29-32, pp. 2059–2071, 2010. DOI: 10.1016/j.cma.2010.03.005.
[55] P. Hao *et al.*, Isogeometric buckling analysis of composite variable-stiffness panels, Compos. Struct., vol. 165, pp. 192–208, 2017. DOI: 10.1016/j.compstruct.2017.01.016.
[56] V. Khalafi and J. Fazilati, Supersonic panel flutter of variable stiffness composite laminated skew panels subjected to yawed flow by using NURBS-based isogeometric approach, J. Fluids Struct., vol. 82, pp. 198–214, 2018. DOI: 10.1016/j.jfluidstructs.2018.07.002.
[57] J. Fazilati and V. Khalafi, Aeroelastic panel flutter optimization of two-steered variable stiffness composite laminated plates using isogeometric analysis, J. Reinf. Plast. Compos., vol. 38, no. 19-20, pp. 885–895, 2019. DOI: 10.1177/0731684419854800.
[58] V. Khalafi and J. Fazilati, Parametric instability behavior of tow steered laminated quadrilateral plates using isogeometric analysis, Thin-Wall. Struct., vol. 133, pp. 96–105, 2018. DOI: 10.1016/j.tws.2018.09.035.
[59] J. Fazilati and V. Khalafi, Effects of embedded perforation geometry on the free vibration of two-steered variable stiffness composite laminated panels, Thin-Wall. Struct., vol. 144, pp. 106287–106287, 2019. DOI: 10.1016/j.tws.2019.106287.
[60] P. Hao *et al.*, Isogeometric analysis and design of variable-stiffness aircraft panels with multiple cutouts by level set method, Compos. Struct., vol. 206, pp. 888–902, 2018. DOI: 10.1016/j.compstruct.2018.08.086.
[61] A. Venkatachari, S. Natarajan, and M. Ganapathi, Variable stiffness laminated composite shells – free vibration characteristics based on higher-order structural theory, Compos. Struct., vol. 188, pp. 407–414, 2018.

Appendix A

[A.1.] Laminates stiffness and inertial terms

$$
\begin{aligned}
&A_{11} = \pi\sum_{n=1}^{nc}\overline{Q}_{11_k}\left(R_n{}^2 - R_{n-1}{}^2\right);\; A_{55} = \frac{\pi}{2}\sum_{n=1}^{nc}\overline{Q}_{55_k}\left(R_k{}^2 - R_{k-1}{}^2\right)\\
&A_{66} = \frac{\pi}{2}\sum_{n=1}^{nc}\overline{Q}_{66_k}\left(R_k{}^2 - R_{k-1}{}^2\right);\; B_{16} = \frac{2\pi}{3}\sum_{n=1}^{nc}\overline{Q}_{16_k}\left(R_k{}^3 - R_{k-1}{}^3\right)\\
&D_{11} = \frac{\pi}{4}\sum_{n=1}^{nc}\overline{Q}_{11_k}\left(R_k{}^4 - R_{k-1}{}^4\right);\; D_{66} = \frac{\pi}{2}\sum_{n=1}^{nc}\overline{Q}_{66_k}\left(R_k{}^4 - R_{k-1}{}^4\right)\\
&I_m = \pi\sum_{n=1}^{nc}\rho_k\left(R_k{}^2 - R_{k-1}{}^2\right);\; I_d = \frac{\pi}{4}\sum_{n=1}^{nc}\rho_k\left(R_k{}^4 - R_{k-1}{}^4\right);\\
&I_p = \frac{\pi}{2}\sum_{k=1}^{nc}\rho_k\left(R_k{}^2 - R_{k-1}{}^2\right)
\end{aligned}
\tag{A.1}
$$

where nc is the number of layers, ρ is the density of material, R_k and R_{k-1} are respectively inner radius and outer radius of the kth layer of the laminated shaft.

[A.2.] The stiffness matrix

$$
[K]^e = \begin{bmatrix}
[K_u]^e & 0 & 0 & 0 & 0 & [K_1]^e\\
0 & [K_v]^e & 0 & [K_2]^e & [K_3]^e & 0\\
0 & 0 & [K_w]^e & [K_4]^e & [K_5]^e & 0\\
0 & [K_2]^{eT} & [K_4]^{eT} & [K_{\beta_x}]^e & [K_6]^e & 0\\
0 & [K_3]^{eT} & [K_5]^{eT} & [K_6]^{eT} & [K_{\beta_y}]^e & 0\\
[K_1]^{eT} & 0 & 0 & 0 & 0 & [K_{\beta_z}]^e
\end{bmatrix}
\tag{A.2}
$$

where

$$[K_u]^e = \frac{1}{L_e} A_{11e} \int_{k_e}^{k_{e+1}} [N'_u]^T [N'_u] d\xi$$
$$[K_v]^e = \frac{1}{L_e} K_{se}(A_{55e} + A_{66e}) \int_{k_e}^{k_{e+1}} [N'_v]^T [N'_v] d\xi$$
$$[K_w]^e = \frac{1}{L_e} K_{se}(A_{55e} + A_{66e}) \int_{k_e}^{k_{e+1}} [N'_w]^T [N'_w] d\xi$$
$$[K_1]^e = \frac{1}{L_e} K_{se} B_{16e} \int_{k_e}^{k_{e+1}} [N'_{\beta_z}]^T [N'_u] d\xi$$
$$[K_2]^e = \frac{1}{L_e} K_{se} B_{16e} \int_{k_e}^{k_{e+1}} [N'_v]^T [N'_{\beta_x}] d\xi$$
$$[K_3]^e = -K_{se}(A_{55e} + A_{66e}) \int_{k_e}^{k_{e+1}} [N'_{\beta_y}]^T [N'_v] d\xi$$
$$[K_4]^e = K_{se}(A_{55e} + A_{66e}) \int_{k_e}^{k_{e+1}} [N'_{\beta_x}]^T [N'_w] d\xi$$
$$[K_5]^e = -\frac{1}{2L_e} K_{se} B_{16e} \int_{k_e}^{k_{e+1}} [N'_w]^T [N'_{\beta_y}] d\xi$$
$$[K_6]^e = \left[\frac{1}{2} K_{se} B_{16e} \int_{k_e}^{k_{e+1}} [N_{\beta_y}]^T [N'_{\beta_x}] d\xi\right] - \left[\frac{1}{2} K_{se} B_{16e} \int_{k_e}^{k_{e+1}} [N_{\beta_x}]^T [N'_{\beta_y}] d\xi\right]$$
$$[K_{\beta_x}]^e = \left[\frac{1}{L_e} D_{11e} \int_{k_e}^{k_{e+1}} [N'_{\beta_x}]^T [N'_{\beta_x}] d\xi\right] + \left[L_e K_{se}(A_{55e} + A_{66e}) \int_{k_e}^{k_{e+1}} [N_{\beta_x}]^T [N_{\beta_x}] d\xi\right]$$
$$[K_{\beta_y}]^e = \left[\frac{1}{L_e} D_{11e} \int_{k_e}^{k_{e+1}} [N'_{\beta_y}]^T [N'_{\beta_y}] d\xi\right] + \left[L_e K_{se}(A_{55e} + A_{66A_{66e}}) \int_{k_e}^{k_{e+1}} [N_{\beta_y}]^T [N_{\beta_y}] d\xi\right]$$
$$[K_{\beta_z}]^e = \frac{1}{L_e} D_{66e} \int_{k_e}^{k_{e+1}} [N'_{\beta_z}]^T [N'_{\beta_z}] d\xi \tag{A.2.1}$$

[A.3.] The mass matrix

$$[M]^e = \begin{bmatrix} [M_u]^e & 0 & 0 & 0 & 0 & 0 \\ 0 & [M_v]^e & 0 & 0 & 0 & 0 \\ 0 & 0 & [M_w]^e & 0 & 0 & 0 \\ 0 & 0 & 0 & [M_{\beta x}]^e & 0 & 0 \\ 0 & 0 & 0 & 0 & [M_{\beta y}]^e & 0 \\ 0 & 0 & 0 & 0 & 0 & [M_{\beta z}]^e \end{bmatrix} \tag{A.3}$$

where

$$[M_u]^e = I_m L_e \int_{k_e}^{k_{e+1}} [N_u]^T [N_u] d\xi$$
$$[M_v]^e = I_m L_e \int_{k_e}^{k_{e+1}} [N_v]^T [N_v] d\xi$$
$$[M_w]^e = I_m L_e \int_{k_e}^{k_{e+1}} [N_w]^T [N_w] d\xi$$
$$[M_{\beta x}]^e = I_d L_e \int_{k_e}^{k_{e+1}} [N_{\beta_x}]^T [N_{\beta_x}] d\xi$$
$$[M_{\beta y}]^e = I_d L_e \int_{k_e}^{k_{e+1}} [N_{\beta_y}]^T [N_{\beta_y}] d\xi [M_{\beta z}]^e = I_p L_e \int_{k_e}^{k_{e+1}} [N_{\beta_z}]^T [N_{\beta_z}] d\xi \tag{A.3.1}$$

where $[N'_j] = \frac{\partial j}{\partial \xi}$, $(j = u, v, w, \beta x, \beta y, \beta z)$